pubs.acs.org/acschemicalbiology

Perspective

Bringing Vibrational Imaging to Chemical Biology with Molecular Probes

Jiajun Du, Haomin Wang, and Lu Wei*

Cite This: *ACS Chem. Biol.* 2022, 17, 1621−1637

Read Online

ACCESS | Metrics & More | Article Recommendations

ABSTRACT: As an emerging optical imaging modality, stimulated Raman scattering (SRS) microscopy provides invaluable opportunities for chemical biology studies using its rich chemical information. Through rapid progress over the past decade, the development of Raman probes harnessing the chemical biology toolbox has proven to play a key role in advancing SRS microscopy and expanding biological applications. In this perspective, we first discuss the development of biorthogonal SRS imaging using small tagging of triple bonds or isotopes and highlight their unique advantages for metabolic pathway analysis and microbiology investigations. Potential opportunities for chemical biology studies integrating small tagging with SRS imaging are also proposed. We next summarize the current designs of highly sensitive and super-multiplexed SRS probes, as well as provide future directions and considerations for next-generation functional probe design. These rationally designed SRS probes are envisioned to bridge the gap between SRS microscopy and chemical biology research and should benefit their mutual development.

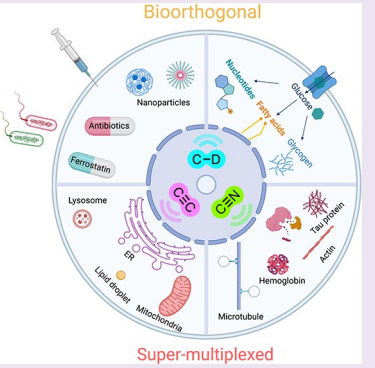

INTRODUCTION

Vibrational spectroscopy, including infrared (IR) absorption and Raman scattering (Figure 1a), reveals molecular information through probing the inherent vibrations of chemical bonds. It has been extensively used for characterizing molecules,[1] deciphering reaction mechanisms,[2,3] and interpreting molecule−environment interactions.[4,5] Raman spectroscopy was first discovered by the physicist Sir C. V. Raman in 1928, where the inelastic Raman scattering shifts a very small portion of photons to lower frequencies upon interacting with molecules.[6] The changes of the photon energy reflect the vibrational energy levels of the chemical bonds within the molecules and thus carry rich chemical information. Although both IR and Raman spectroscopy contain vibrational information of the molecules, they have different selection rules. For example, water has very high IR absorption but weak Raman scattering. In addition, Raman typically utilizes UV to near-infrared light (200−1100 nm), while IR relies on mid-infrared light (2500−50000 nm); thus the spatial resolution (scaling inversely with the light wavelength) is much higher for Raman (Figure 1a). Both the subcellular spatial-resolution and the minimal water background make Raman scattering a better-suited technique for biological imaging.

However, the utility of spontaneous Raman is largely limited by its feeble signals ($\sim 10^{10}$ smaller than fluorescence), which requires a long acquisition time and is easily overwhelmed by the autofluorescence background from biological samples. To address both issues, coherent anti-Stokes Raman scattering (CARS) microscopy (Figure 1a) was invented. CARS microscopy significantly boosts the imaging sensitivity and speed and pushed Raman spectromicroscopy to be more compatible with biological imaging.[7] However, CARS signals suffer from severe nonresonant backgrounds and have nonlinear concentration dependence, which sacrifices imaging quality and adds complexity for imaging annotation.[8] Around 2008, stimulated Raman scattering (SRS) microscopy was introduced, providing even better sensitivity than CARS and tackling the issues present with CARS.[9−11] SRS utilizes two spatially and temporally overlapped laser pulse trains (pump and Stokes, Figure 1b), which enhances the otherwise weak Raman transitions by up to 10^8-fold through stimulated emission quantum amplification. This two-photon excitation feature also yields SRS intrinsic 3D optical sectioning capability for deep tissue imaging. In addition, the technical implementation of the high-frequency modulation transfer scheme also pushes the detection sensitivity of SRS close to the theoretical limit and removes the potential fluorescence and other interfering background. The readers are encouraged to check more technical details of SRS in other reviews.[12,13]

It is now widely recognized that SRS is the most suitable far-field Raman imaging modality for live biological studies with provided image quality comparable to fluorescence micros-

Received: March 6, 2022
Accepted: June 24, 2022
Published: June 30, 2022

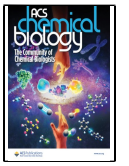

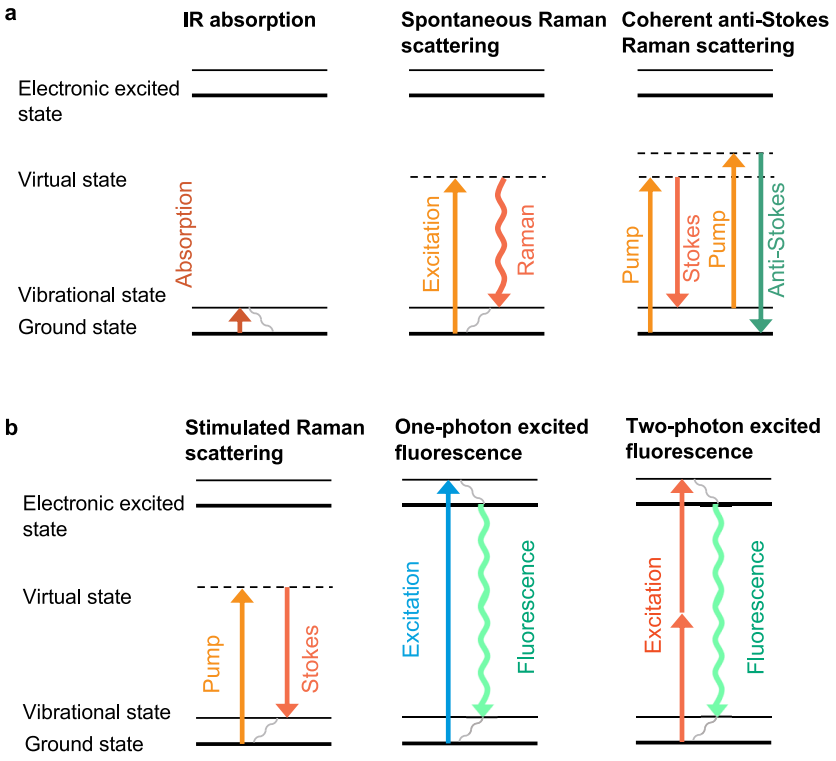

Imaging modality	Stimulated Raman scattering microscopy	One-photon fluorescence microscopy	Two-photon fluorescence microscopy
Contrast origins	Chemical bonds	Fluorophores	Fluorophores
Electronic excitation	No	Yes	Yes
Lasers	Picosecond or femtosecond pulsed laser	CW laser	Femtosecond pulsed laser
Power dependence	$\propto I_{pump}I_{Stokes}$	$\propto I_{ex}$	$\propto I_{ex}^2$
Compatible samples	Fixed or live samples	Fixed or live samples	Fixed or live samples
Pixel dwell time	μs	μs	μs
Spatial resolution	300-500 nm (lateral) 1-2 μm (axial)	200-300 nm (lateral) ~1 μm (axial)	300-600 nm (lateral) 1-2 μm (axial)
Sensitivity	mM for endogenous species; μM for triple-bond probes; nM for pre-resonance MARS dyes and the polyynes;	Up to single-molecule	Up to single-molecule
Intrinsic 3D sectioning capability	Yes	No	Yes
Imaging depth in brain tissues	200-500 μm	50-100 μm	300-500 μm
Probe quenching/photobleaching	Minimum	Yes	Yes
Hyperspectral information	Yes	Limited	Limited

Figure 1. Energy diagrams of different vibrational micro-spectroscopy and fluorescence microscopy. (a) Energy diagrams of IR absorption, spontaneous Raman scattering, and CARS spectroscopy. (b) Energy diagrams and key parameters of SRS microscopy and one- and two-photon excited fluorescence microscopy.[13,20−23]

https://doi.org/10.1021/acschembio.2c00200
ACS Chem. Biol. 2022, 17, 1621−1637

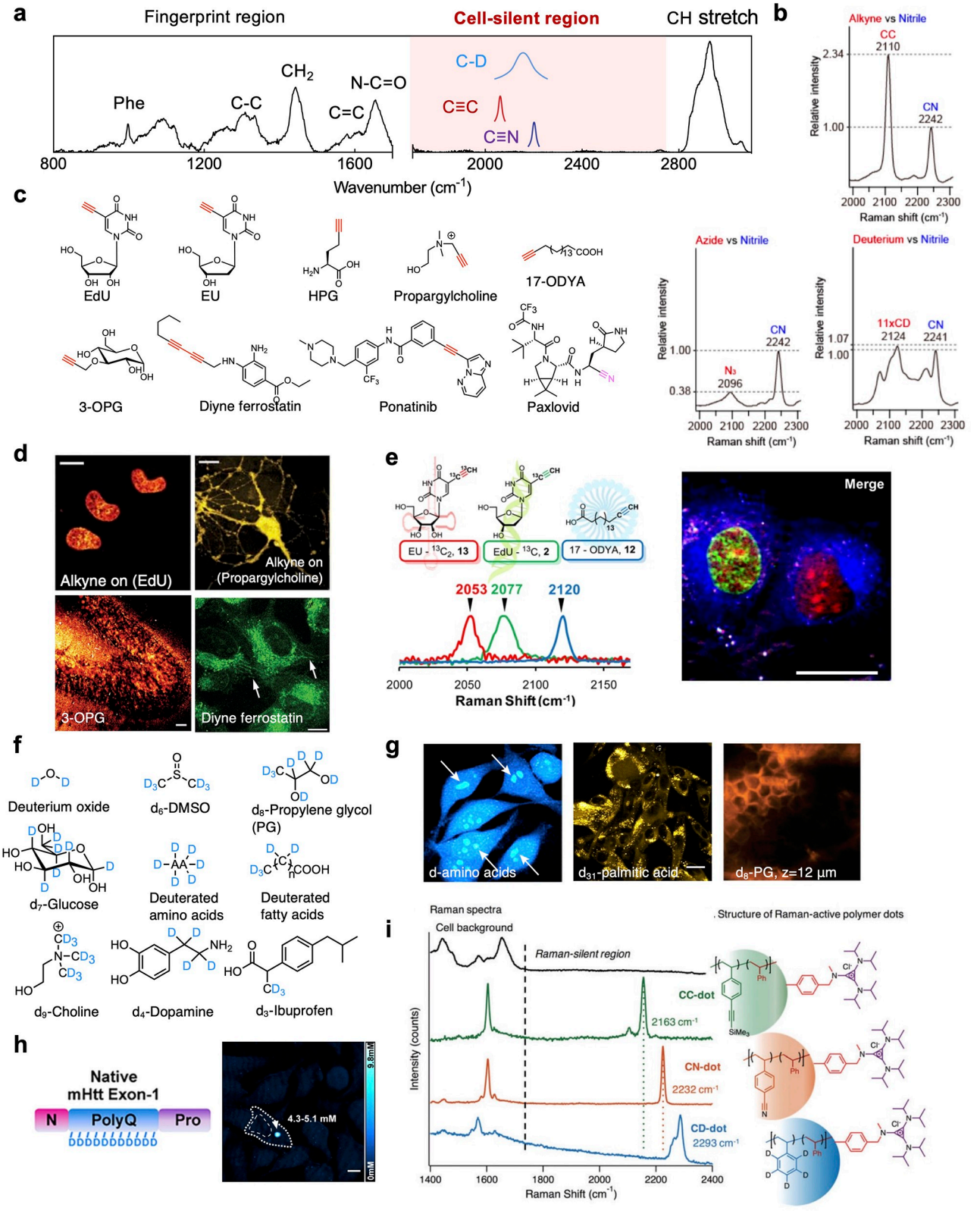

Figure 2. Small biorthogonal Raman tagging with C≡C, C≡N, and C—D. (a) Typical Raman spectrum of a mammalian cell (on glass slides) depicting the crowded fingerprint region, the C—H stretch region, and the cell-silent region (pink). (b) Relative Raman peak intensities of common silent-region Raman tags (i.e., C≡C, C≡N, and C—D). Adapted in part with permission from ref 64. Copyright 2012 American Chemical Society. (c) Representative triple-bond tagged small metabolites and drugs. (d) SRS imaging targeting the alkyne vibrations for incorporation of thymidine-analogue EdU in live HeLa cells, choline-analogue propargylcholine in live neurons, glucose-analogue 3-OPG in cultured mouse brain tissue slices (scale bar 40 μm), and alkyne-tagged ferrostatin in live HT-1080 cells. Other scale bars 10 μm. Adapted in part with permission from ref 32. Copyright 2014 Nature Publishing Group. Adapted in part with permission from ref 65. Copyright 2015 Wiley-VCH Verlag GmbH & Co. KGaA, Weinheim. Adapted in part with permission from ref 59. Copyright 2018 American Chemical Society. (e) ^{13}C isotope

https://doi.org/10.1021/acschembio.2c00200
ACS Chem. Biol. 2022, 17, 1621−1637

Figure 2. continued

editing enables three-color imaging of EdU, EU, and 17-ODYA with alkyne probes. Scale bar 25 μm. Adapted in part with permission from ref 61. Copyright 2014 American Chemical Society. (f) Representative small molecules with deuterium tagging. (g) SRS imaging targeting the C—D vibration for the incorporation of deuterated amino acids in live HeLa cells, d_{31}-palmitic acid in melanoma cells (scale bar 20 μm), and d_8-PG in the mice stratum corneum at a depth of 12 μm after 124 min of treatment. Adapted in part with permission from ref 66. Copyright 2013 United States National Academy of Sciences. Adapted in part with permission from ref 29. Copyright 2020 Nature Publishing Group. Adapted in part with permission from ref 67. Copyright 2014 American Chemical Society. (h) SRS imaging of d_5-Gln-labeled mHtt-97Q aggregates in live HeLa cells. Quantifications for the local polyQ concentrations within the aggregates are also shown. Scale bar 10 μm. Adapted in part with permission from ref 68. Copyright 2020 American Chemical Society. (i) C—D and triple-bond enriched polymer dots with amplified Raman signals. Adapted in part with permission from ref 69. Copyright 2017 The Royal Society of Chemistry.

copy. Prominently, SRS also achieved high imaging speed up to video-rate (110 frames/s)[14−16] and a spatial resolution within 100 nm with recent instrumentation and sample-expansion strategies.[17−19] It would be informative to compare the key technical and application features of SRS microscopy with the popular one- and two-photon fluorescence microscopies. We provide the energy diagrams and a table summarizing key imaging parameters for the three techniques in Figure 1b. Compared to fluorescence microscopy, the absence of electronic excitation provides SRS with general imaging capability of all types of molecules with minimum photobleaching or environmental quenching. In addition, SRS typically uses near-infrared excitation lasers (800−1100 nm) and thus offers less phototoxicity compared to one-photon fluorescence with visible laser excitation. This near-infrared excitation together with the intrinsic 3D sectioning makes the penetration depth of SRS similar to that obtained by two-photon fluorescence, suitable for imaging thick tissues. Moreover, the common utilization of picosecond lasers in SRS renders a much smaller laser peak power compared to that from femtosecond lasers for two-photon fluorescence, resulting in less nonlinear photodamage. However, the micromolar to millimolar detection sensitivity is still the major challenge in SRS that limits its application for detecting molecules with low abundance in live biological samples. Recent developments in probe engineering such as the creation of highly sensitive MARS and polyyne dyes has largely improved the sensitivity of SRS down to nanomolar and broken the traditional color barrier in fluorescence microscopy with super-multiplexed imaging.

LABEL-FREE VIBRATIONAL IMAGING

Since Raman signals originate from chemical bonds instead of conjugated fluorophores, SRS offers general imaging applicability for versatile molecules. Since its inception, SRS microscopy has established itself as a powerful label-free bioimaging modality. Targeting the fingerprint region (500−1700 cm^{-1}) or high wavenumber carbon−hydrogen (C—H) stretching region (2800−3100 cm^{-1}), nucleic acids, proteins, lipids, carbohydrates, neurotransmitters, and other endogenous biomolecules carrying O—P—O, C═O, C═C, C—H_2, and C—H_3 bonds are readily imaged with subcellular resolution (Figure 2a). Additionally, hyperspectral SRS[24,25] adds another layer of information for subcellular spectral analysis. With these capabilities, label-free SRS paves the way for various applications, including sensing environmental cues,[26] studying lipid metabolism and identifying druggable targets,[27−31] tracking drug delivery and distribution,[10,32−34] multicolor cell sorting,[35,36] fast diagnosis of tumors,[37,38] and investigation of amyloid plaques in neurodegenerative diseases.[39,40] The current imaging speed, throughput, and detection sensitivity are still being continuously improved with rapid instrumental innovations.[41−43] In parallel, emerging data processing approaches, particularly machine learning algorithms, further upgrade image quality and enable data mining with rich chemical information.[18,29,43−45]

Despite the success of label-free SRS imaging, there are several fundamental limitations. First, the specificity of targets is often compromised since endogenous biomolecules tend to share multiple chemical bonds and therefore overlapping spectra. Second, the detection limit of SRS is still relatively low compared with fluorescence, at the scale of millimolar for most biomolecules. Thus, label-free SRS is more suited for investigating relatively abundant molecules including proteins, lipids, nucleic acids, and carbohydrates. Third, label-free imaging is not capable of tracking many dynamic processes such as uptake, synthesis, catabolism, and intracellular-to-extracellular interactions. These limitations largely restrict the applications of SRS imaging but can be greatly diminished through the implementation of Raman probes.

LABELING WITH BIOORTHOGONAL PROBES

Driven by the need for higher specificity, sensitivity, and functionality, which are fundamentally limited in the label-free approaches, Raman labels have been introduced to shift SRS imaging from the label-free to the labeling paradigm.[46] Fortunately, the cell-silent spectral region (1800−2800 cm^{-1}), where there are no endogenous Raman signals from cells, leaves spacious spectral room for background-free Raman labeling and imaging (Figure 2a). Bioorthogonal chemical bonds, including alkynes (C≡C), nitriles (C≡N), and carbon−deuterium bonds (C—D) are small, nontoxic, and Raman active in this clean region, making them well suitable for tagging with low perturbation to the biological systems.[46] As such, biorthogonal SRS is especially beneficial for live-cell interrogations of small molecules including metabolites and drugs whose label-free vibrational signatures are overwhelmed by cellular background and whose physiological functions are perturbed by conventional fluorophore labeling.

Furthermore, by harnessing the narrow line width of Raman peaks (50−100 times narrower than fluorescence peaks), researchers have developed highly sensitive Raman probe palettes. The matching dye palettes enable super-multiplexed (more than 20 channels) optical imaging for organelles or protein profiling with sensitivity down to 250 nM, bridging optical imaging's subcellular spatial resolution with system biology's high information throughput.[47−49] Moreover, chemically activatable and photochromic SRS probes have also been developed lately for intracellular sensing and multiplexed tracking, empowering functional SRS imaging.[50−54]

All these recently established Raman probes have greatly expanded the application boundary of vibrational imaging.

https://doi.org/10.1021/acschembio.2c00200
ACS Chem. Biol. 2022, 17, 1621−1637

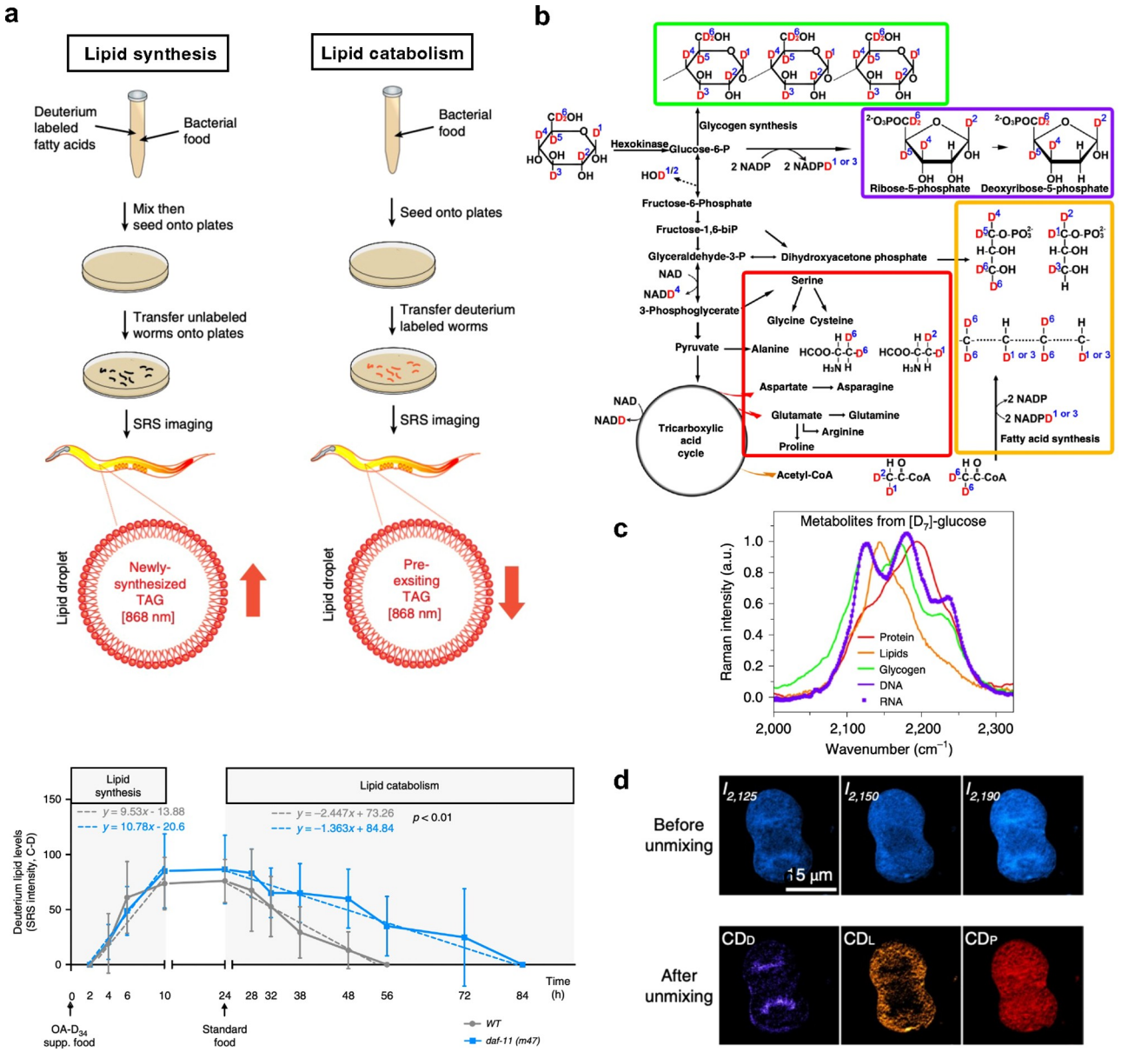

Figure 3. Metabolic pathway analysis with deuterium labeling. (a) Utilizing SRS imaging assays to determine the rate of lipid synthesis (left) and lipid mobilization (right) with deuterium-labeled fatty acids in *C. elegans*. Signals derived from deuterium-labeled lipids in intestinal lipid droplets were quantified (bottom); daf-11 mutants have similar rates of lipid synthesis but with reduced rates of lipid catabolism. Adapted in part with permission from refs 83 and 84. Copyright 2017 and 2020 Nature Publishing Group. (b) Biological pathways from d_7-glucose incorporation for spectral tracing of deuterium isotopes (STRIDE) of various metabolic products. Adapted in part with permission from ref 85. Copyright 2019 Nature Publishing Group. (c) Normalized C—D Raman spectra of five d_7-glucose-derived biomolecules, including proteins, lipids, glycogen, DNA, and RNA. Adapted in part with permission from ref 85. Copyright 2019 Nature Publishing Group. (d) Images of a d_7-glucose metabolically labeled mitotic HeLa cell before and after spectral unmixing. Adapted in part with permission from ref 85. Copyright 2019 Nature Publishing Group.

Efforts in the past decade have proven that probe development plays a central role in driving the next frontiers of SRS microscopy. The growing chemical biology toolbox inspires the development of new SRS imaging functionalities. In turn, the SRS platform also finds a unique niche for chemical biology studies. Exploring new opportunities for merging SRS imaging with chemical biology is worth brainstorming. In this perspective, we first review recent notable advances in the development of Raman probes and their biological applications. On this basis, we provide an outlook to further expand multiplexing, enhance Raman signals, and utilize SRS imaging to decipher new biology.

SMALL-MOLECULE RAMAN TAGGING

Triple bonds (e.g., C≡C, C≡N) and stable isotope-substituted chemical bonds (e.g., C—D, N—D, O—D) vibrate in the cell-silent region (Figure 2a). Among these chemical bonds, C≡C has the highest Raman signals (Figure 2b). One representative molecule tagged by C≡C is 5-ethynyl-2′-deoxyuridine (EdU), the widely adopted thymidine analogue with an SRS detection limit of 200 μM,[32] and it is now frequently used as a benchmark for Raman intensity quantification. Pioneered by the click chemistry field, chemists have developed a suite of alkyne-tagged molecular handles for biolabeling, many of which can now be directly detected by

https://doi.org/10.1021/acschembio.2c00200
ACS Chem. Biol. 2022, 17, 1621−1637

Raman without the subsequent click reactions. With these available and newly developed Raman-tailored alkyne probes (Figure 2c), dynamic metabolic processes including DNA synthesis and choline and glucose uptake can be readily visualized in live cells and tissues (Figure 2d with the corresponding analog structures shown in Figure 2c).[32,55−59] Additionally, drugs bearing native alkynes (e.g., ponatinib) or nitriles (e.g., paxlovid) or ones subjected to proper alkyne derivatization such as diyne-ferrostatin (Figure 2c,d) can be quantitatively imaged for intracellular distribution with well-maintained pharmacokinetics.[32,59,60] Inspired by the colorful fluorescent protein palette, alkyne "vibrational colors" are also tunable through an isotope-editing strategy based on the dependence of Raman frequency on the bond mass. A set of ^{13}C-edited probes were developed that enabled multicolor SRS imaging of DNA, RNA, and lipids in the same set of live cells[61] (Figure 2e).

Compared to C≡C, C≡N has lower (about 40%) Raman cross sections (Figure 2b). However, as the peak frequencies of C≡N are sensitive to the physical environment (particularly the electrostatic interactions[4,62,63]), they provide additional functions as vibrational sensors. Additionally, the C≡N vibration occupies a higher frequency region (2200−2300 cm^{-1}), which separates well from that of C≡C (2100−2200 cm^{-1}). Therefore, nitriles with similar isotope-editing for frequency shifting could be combined with alkynes for expanded imaging multiplexing.

Deuterium (the stable isotope of hydrogen)-labeled chemical bonds (exemplified by the C—D) have unmatched advantages. Most importantly, since stable isotopes have almost the same physicochemical properties as their counterparts, the labeled molecules could be processed by cells' natural machineries with minimal perturbation to the native biological functions. In addition, compared to the label-free imaging of C—H, C—D yields improved SRS detection limit due to the absence of interfering cellular background. Although the Raman cross section of C—D is smaller than that of the triple bonds (Figure 2b), what is lacking in cross section could be compensated by the large labeling number. For example, palmitic acid, the most common long-chain saturated fatty acid in mammalian cells, can have up to 31 deuterium atoms per molecule as d_{31}-palmitic acid. Owing to these features, deuterium plays a significant role in Raman labeling and has been applied to interrogating a wide range of uptake and metabolic dynamics for targets including amino acids,[66] glucose,[70] fatty acids,[71] choline,[72] cholesterol,[73] water,[74] solvents,[33] and drugs[67] (Figure 2f). For instance, the employment of deuterated amino acids allows imaging of complex protein metabolism, including synthesis, degradation, and analysis of temporally defined populations[66] (Figure 2g). Similarly, d_{31}-palmitic acid enabled quantitative visualization of fatty acid uptake and metabolic incorporation;[29] and the deuteration of propylene glycol (PG) allowed the capture of real-time 3D penetration for this common pharmaceutical cosolvent or excipient across the mouse stratum corneum[67] (Figure 2g).

Deuterium labeling can also achieve protein-specific imaging in live cells for certain targets. For example, the aggregation-prone mutant Huntington (mHtt) protein harboring polyglutamine (polyQ) expansions has been shown to be specifically labeled by deuterated glutamine for enrichment in the polyglutamine expansions[68] (Figure 2h). This approach enabled the first quantitative analysis of mHtt and non-mHtt proteins inside the same protein aggregates in live cells without the need for any fluorescent labels. To expand the library of labeled targets apart from proteins, similar selective labeling strategies may be developed, such as the selective labeling of glycogen by deuterated glucose in live cancer cells.[75] The concept of harnessing such repeating units toward higher sensitivity was also adopted for C—D and triple-bond containing polymers, which could amplify the Raman signals by up to 10^5-fold[69,76−79] (Figure 2i). The versatile applications of Raman-tagged cellular imaging are still expanding and would benefit from facile synthesis of new vibrationally tagged molecules. Toward this front, we envision that the recent synthetic advances in late-stage functionalization[80−82] could provide convenient synthetic routes to deuterium or triple-bond tagged molecular targets beyond currently available pools.

METABOLIC PATHWAY ANALYSIS WITH DEUTERIUM LABELING: FROM CELL METABOLISM TO MICROBIOLOGY

Various small Raman labels offer a wide range of applicability especially for investigating different aspects of cellular metabolism. To assay the uptake of metabolites (e.g., glucose), triple bonds are usually the top choice for their higher detectability.[57,65] However, even triple-bond tagged metabolic analogs usually stop at the early catabolic steps in the metabolic pathway. In this case, stable isotope tagged metabolites are superior for tracing transformations into the downstream metabolic products from live cells to organisms with minimum toxicity.[13] For example, with deuterated fatty acid labeling, lipid synthesis, and mobilization could be noninvasively probed in live *C. elegans* by SRS with high throughput[83,84] (Figure 3a). *C. elegans* with daf-11 mutations were discovered to have no changes in the rate of lipid synthesis but a significant reduction in the rate of lipid catabolism.[84]

Comprehensive cellular metabolism beyond metabolite uptake or distribution can be probed with suitable deuterium labeled probes. Glucose is the primary energy source for mammalian cells as well as an important precursor of downstream metabolites including amino acids, lipids, nucleic acids, glycogen, and adenine dinucleotide phosphate (NADPH).[86] While 3-*O*-propargyl-D-glucose (3-OPG, i.e., alkyne-tagged glucose, Figure 2d) is able to capture the glucose uptake in live cells and tissues, it stops at the phosphorylation step when going into the glucose metabolism pathway.[61] Recently, with deuterated glucose (i.e., d_7-glucose) labeling, diverse downstream products, such as DNA/RNA, proteins, lipids, and glycogen, have been shown to be sparsely labeled with deuterium through each corresponding metabolic pathway[85] (Figure 3b). These sparsely labeled downstream products are spectrally separable with varied features due to the different chemical environments surrounding the deuterium (Figure 3b,c).[70,75,85] A linear combination algorithm can then be utilized to quantitatively retrieve the relative C—D enrichment maps in each identified species[75,85] (Figure 3d). Alternatively, site-specific deuterated glucose, instead of d_7-glucose, allows for tracing specific metabolic pathways. For example, 3-D-glucose ([3-D]Glc) was shown to monitor NADPH-mediated lipid synthesis through the oxidative pentose phosphate pathway (oxPPP) by targeting lipid droplets.[88]

https://doi.org/10.1021/acschembio.2c00200
ACS Chem. Biol. 2022, 17, 1621−1637

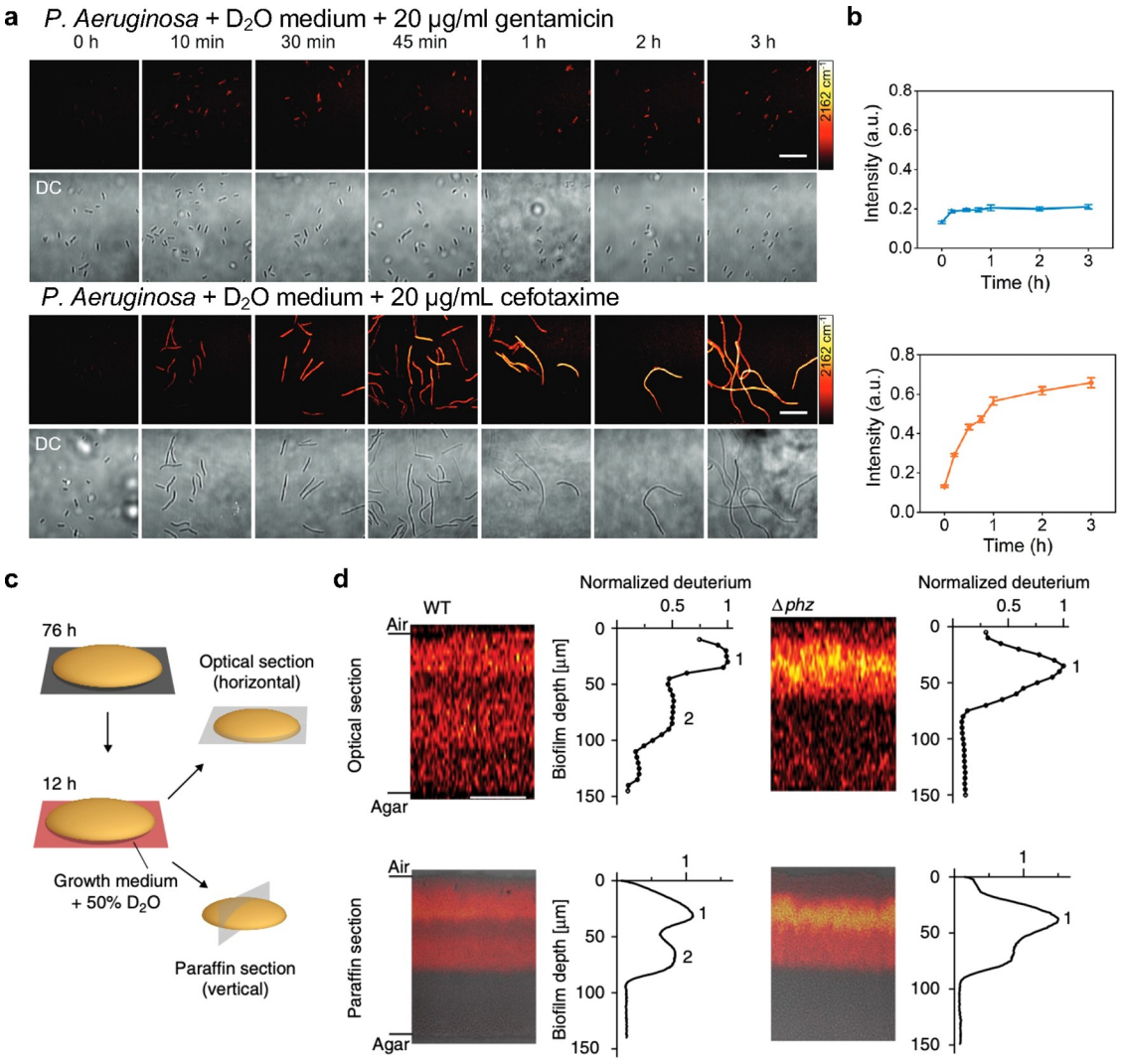

Figure 4. Assaying microbial metabolism with the biorthogonal SRS platform. (a) Time-lapse SRS (targeting the C—D vibration, 2162 cm^{-1}) and the corresponding transmission imaging of *P. aeruginosa* after culturing in D_2O-containing medium with the addition of 20 μg mL^{-1} gentamicin (top) or cefotaxime (bottom). Scale bars 20 μm. Adapted in part with permission from ref 89. Copyright 2020 Wiley-VCH Verlag GmbH & Co. KGaA, Weinheim. (b) Corresponding average C—D intensity plot (designating labeled biomass) over time for *P. aeruginosa* after culturing in D_2O-containing medium with gentamicin (top, blue) or cefotaxime (bottom, orange) treatment. Number of cells, $N \geq 10$ per group. Error bars indicate SEM. Adapted in part with permission from ref 89. Copyright 2020 Wiley-VCH Verlag GmbH & Co. KGaA, Weinheim. (c) Schematic of two methods to visualize metabolic activity in colony biofilms. Optical sectioning uses the inherent 3D sectioning capability of SRS to acquire images in *z*-direction in 5 μm steps without sample preparation procedure. The paraffin section requires paraffin embedding and sectioning to provide 10 μm thin slices for imaging. Adapted in part with permission from ref 90. Copyright 2019 Nature Publishing Group. (d) SRS images and the corresponding plots of deuterium signals per biofilm depth for both optical sections and paraffin sections of colony *P. aeruginosa* biofilms after a 12 h incubation in D_2O-containing medium. Data plots show the mean deuterium signal per biofilm depth. One replicate each of WT and Δ*phz* is shown and is representative of at least five biological replicates. Scale bars 50 μm. Adapted in part with permission from ref 90. Copyright 2019 Nature Publishing Group.

Metabolic reprogramming serves as a unique hallmark for cancer and neurodegenerative diseases. This Raman-based imaging platform for complex glucose metabolism hence forms a live-cell spatially resolved assay with subcellular resolution. Indeed, cancer cells have been shown to exhibit different levels of glucose uptake rate versus metabolism rate.[87] Subcellular glycogen accumulation through d_7-glucose labeling was also discovered in cancer cells as a potential indicator for their resistance to glucose deficiency.[75] A similar spectral tracing strategy can be applied to cost-effective heavy water labeling (DO-SRS).[74] Since water is the most abundant molecule in biological systems, the incorporation of deuterium from D_2O to C—D in macromolecules is highly efficient even at low and biologically safe D_2O concentrations (e.g., 20% D_2O). The resulting distinct spectral signatures of C—D enable visualization of both lipid and protein metabolism in animals with long-term incubation (26 days).[74]

Microbiology is another application field that can be empowered by the metabolic Raman platform. The role of microbiota is increasingly recognized in human health. One of the most important problems associated with microbes is antibiotic resistance. Current standard antimicrobial susceptibility testing (AST) requires 16−24 h for multiple cell cycle growth. By culturing the microbes in 70% D_2O medium and tracing the metabolic incorporation of deuterium into the biomass, one can probe varied metabolic responses to

https://doi.org/10.1021/acschembio.2c00200
ACS Chem. Biol. 2022, 17, 1621−1637

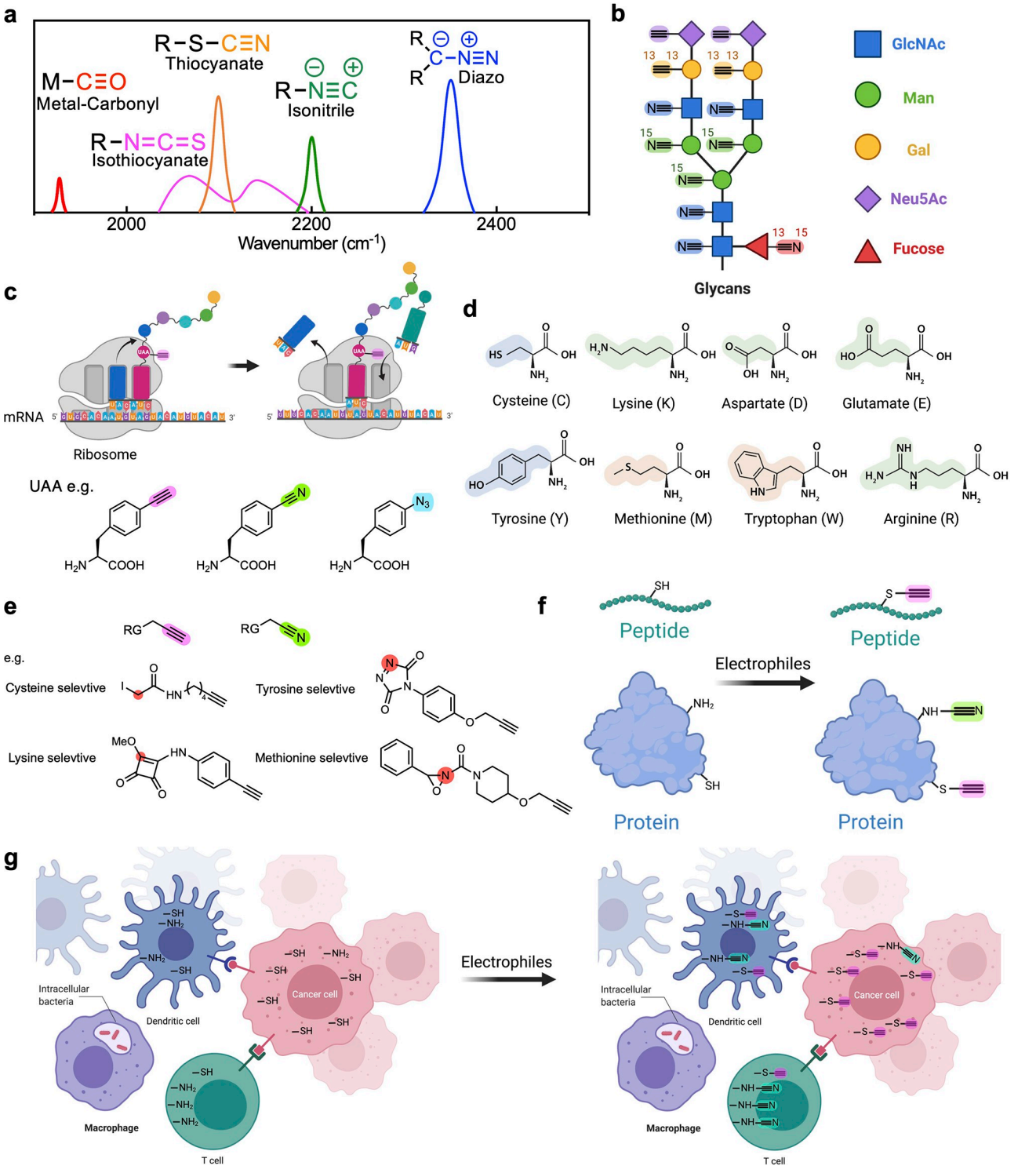

Figure 5. Proposed applications for SRS imaging with small tagging. (a) Additional triple bonds for SRS imaging that vibrate in the cell-silent region (the spectral features of these additional triple bonds are based on the reference compounds including $Mn(tpm)(CO)_3Cl$ (metal−carbonyl), benzyl isothiocyanate (isothiocyanate), 4-bromobenzenediazonium tetrafluoroborate (diazo), benzyl isocyanide (isonitrile), and benzyl thiocyanate (thiocyanate)). (b) Spatial glycan profiling with triple bond labeled monosaccharides. (c) Genetically encoded protein labeling using unnatural amino acids (UAA) with triple bonds. (d) Representative nucleophilic amino acid residues. (e) Representative triple-bond containing electrophiles that target specific amino acid residues. RG, reaction group. Red circles indicate the initial site of electrophilic reactivity. (f) Site-specific peptide and protein labeling with amino-acid selective electrophiles (exemplified in panel e). (g) Potential spatial mapping for the reactivity of specific amino acid residues in complex biological systems with selective triple bond containing electrophiles (exemplified in panel e).

antibiotics in as short as 10 min, the fastest method to date.[89] The C—D signals indicated that *Pseudomonas aeruginosa* (*P. aeruginosa*), a common cause of hospital-acquired infection, exhibits distinct metabolic rates under different common antibiotic (gentamicin and cefotaxime) treatments (Figure 4a,b). As such, SRS imaging provides a rapid and cost-effective

https://doi.org/10.1021/acschembio.2c00200
ACS Chem. Biol. 2022, 17, 1621−1637

AST assay. In a more clinically relevant *P. aeruginosa* biofilm system, 3D metabolic activity deep inside the film was visualized by SRS with 50% D_2O medium labeling.[90] SRS's inherent optical sectioning capability provides a convenient way to visualize 3D metabolic activity without the need for traditional paraffin embedding and sectioning (Figure 4c). The active metabolism in the hypoxic deep region was revealed to be supported by the small redox metabolite phenazine (phz) in the optical sections[90] (Figure 4d(top), WT vs Δ*phz*, peak 2). This finding was validated by paraffin sections ((Figure 4d(bottom), WT vs Δ*phz*, peak 2). In different *Staphylococcus aureus* biofilms, tagging antibiotic vancomycin with alkynes uncovered a nonuniform and limited penetration of antibiotic into the biofilm with preferential affinity of the antibiotic to the cells instead of the extracellular polymeric matrix (EPM).[91]

PROPOSAL FOR SRS IMAGING WITH SMALL TAGGING

The coupling of SRS with small vibrational tags has established itself as a powerful live-cell imaging platform. Going beyond what has been achieved, herein we discuss some of our thoughts for further improvements of molecular probes and potential opportunities of the platform in chemical biology. First, the wide cell-silent region remains spacious with room for spectral multiplexing (Figure 2a). Other triple bonds (Figure 5a), including metal−carbonyl (M—C≡O),[92] isothiocyanate (—N═C═S), diazo (—N≡N), isonitrile (—N≡C), and thiocyanate (—S—C≡N), with strong vibrations in this region are worth in-depth investigations and engineering for their biological utilities. If these additional tags are available, the multiplexing of Raman-based profiling strategies could be greatly expanded. New applications, such as imaging-based glycan profiling of cells, could then be envisioned. Glycans are oligosaccharides attached to biomacromolecules including proteins. They are regarded as post-translational modifications for modulating cell functions but are still less understood due to the lack of methods for studying them.[93] A typical way to image glycan directly from cells is through metabolic incorporation of unnatural monosaccharides with small chemical reporters (e.g., azides or alkynes), which undergo sequential labeling via biorthogonal chemistry.[94] However, vastly different kinetics and selectivity and the scarce availability of the biorthogonal reactions limit the applicability of multiplexed monosaccharide labeling. With SRS imaging, we envision that spatial glycan profiling of monosaccharides covering *N*-acetylglucosamine (GlcNAc), mannose (Man), galactose (Gal), sialic acid (Neu5Ac), and fucose in live systems will be possible with proper isotope-edited triple-bond tagging (Figure 5b) together with the expandable tag repertoire (Figure 5a).

In addition to metabolic labeling, site-specific labeling through genetic encoding, such as utilizing unnatural amino acids (UAAs) with genetic code expansion (Figure 5c), is another direction that is worth exploring for protein-selective Raman imaging. Although numerous UAAs carrying alkynes or nitriles have been developed (Figure 5c),[62,95] SRS signals from these single-UAA labeled proteins are not sufficient.[96] While technical innovations are in urgent need of sensitivity improvement,[42] new chemical or biological labeling strategies to incorporate an increased number (>10) of triple bonds in one protein would also be a breakthrough for obtaining satisfying SRS signals for general protein imaging applications. Toward higher sensitivity, aqueous Glaser−Hay bioconjugation,[97] which may extend the terminal alkynes from UAAs into polyynes *in situ*, could be an alternative option to reduce the required labeling number of UAAs by serving as a sequential signal-amplification method.

Compared to fluorophores, these small and multiplexed triple-bond Raman tags allow wider accessibility due to much smaller tag sizes and require no sequential labeling (e.g., click reaction) for highly multiplexed applications. We hence expect that SRS imaging will contribute to solving certain important chemical biology questions, such as spatially resolving the proteome reactivity in live cells. The side chain reactivity of canonical amino acids together with the local protein microenvironment builds up "hotspots" in the proteome.[98] The electron-rich side chains of various amino acids including cysteine, lysine, aspartate, glutamate, tyrosine, and methionine are natural targets for electrophiles (Figure 5d). These functional amino acids are always catalytic residues or sites of post-translational modifications, and thus they are the keys for modulating cellular functions. The side-chain reactivity of the amino acids can be quantitatively analyzed with the isotopic tandem orthogonal proteolysis activity based protein profiling (isoTOP-ABPP) platform.[98,99] This mass spectrometry method has high throughput and unmatched protein resolvability, but it lacks spatial information and cannot track dynamic processes with intra- and intercellular interaction in complex biological systems.

Recently, researchers comprehensively profiled the proteome-wide reactivity for a library of 54 alkyne-bearing electrophiles.[100] They identified highly selective probes that specifically conjugate to a total of 9 amino acids plus the N-terminus with different reactivities (several representative probes are listed in Figure 5e). These alkyne-tagged electrophiles provide an effective site-selective labeling tool for proteins or peptides (Figure 5f). The alkyne handles across these electrophile probes (Figure 5e) could be substituted with color-resolvable isotope-labeled triple bonds from the Raman probe repertoire (Figure 5a,b). With this design, it is possible to generate maps for amino acid reactivities in a complex biological system such as cancer immunology and microbe−host environment. Upon supplying the probes into the systems, the subsequent multiplexed SRS imaging would allow single-cell profiling *en masse* (Figure 5g). Sufficient signals should be expected with this strategy since similar proteome-wide new protein synthesis using alkyne-tagged methionine (homopropargylglycine (HPG), Figure 2c) labeling was already demonstrated by SRS imaging in live cells.[32] This application would be highly challenging for direct fluorescent labeling as the active amino acid residues are likely less accessible to bulkier fluorophores without the sequential labeling step. Together with isoTOP-ABPP and protein targeting labeling, proteome-wide SRS screening may contribute to annotating specific proteins and elucidating their spatially resolved dynamic activity changes.

NEXT-GENERATION RAMAN PROBE PALETTES FOR HIGHLY SENSITIVE AND SUPER-MULTIPLEXED IMAGING

Even with signal amplification from SRS and the introduced Raman tags, there is still a sensitivity gap between SRS and fluorescence microscopy. The SRS detection limit of EdU is 200 μM in live cells, while the most sensitive fluorophores offer single-molecule sensitivity (<10 nM). One central drive in SRS imaging is to narrow this sensitivity gap. A promising solution

https://doi.org/10.1021/acschembio.2c00200
ACS Chem. Biol. 2022, 17, 1621−1637

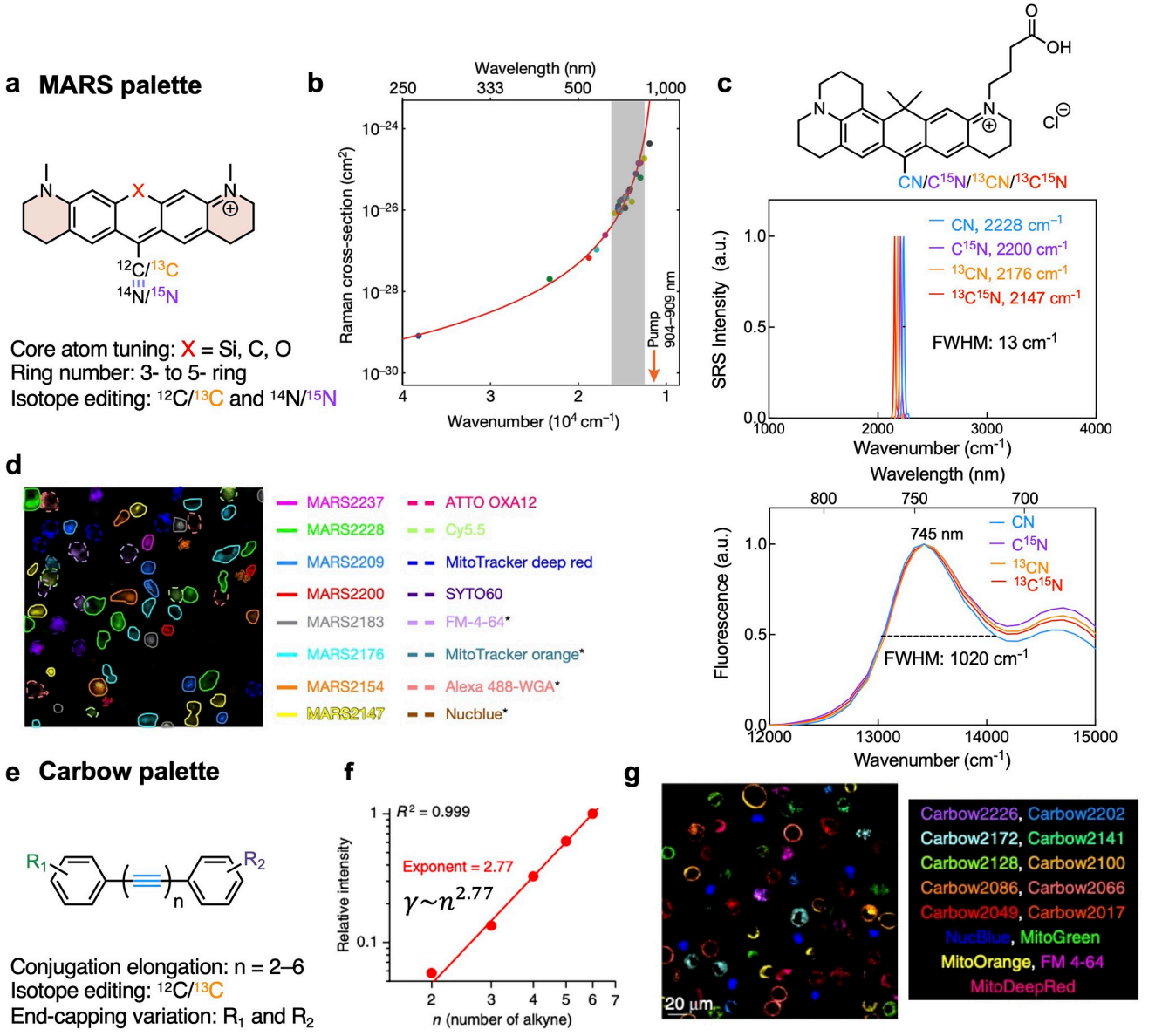

Figure 6. Physical principles for the current design of strong and super-multiplexed Raman probes. (a) Construction of 24-color MARS xanthene palette. (b) Dramatic increase of SRS cross sections by electronic preresonance enhancing effects. Adapted in part with permission from ref 47. Copyright 2017 Nature Publishing Group. (c) The nitrile SRS peaks (top) and fluorescence absorption spectra (bottom) of a series of four isotope labeled MARS dyes (structure drawn at the top). The full width half-maximum (fwhm) of the nitrile SRS peaks and the dominant absorption peaks are listed. (d) Live-cell 16-color imaging with MARS and commercial dyes. Adapted in part with permission from ref 47. Copyright 2017 Nature Publishing Group. (e) Construction of 20-color Carbow polyyne palette. (f) Superlinear (an exponent of 2.77) SRS-signal growth with the number of conjugated alkynes. Adapted in part with permission from ref 104. Copyright 2018 Nature Publishing Group. (g) Live-cell 15-color imaging with Carbow and commercial dyes. Adapted in part with permission from ref 104. Copyright 2018 Nature Publishing Group.

that has been proven successful is the development of highly sensitive Raman probes. As the Raman bands are inherently narrow (peak width about 10 cm^{-1}, ~50−100 times narrower than fluorescent peaks), these Raman probes would enable high-throughput super-multiplexed (>20 channels) imaging once the requirement for sensitivity is met. Therefore, Raman imaging holds the promise of breaking the color barrier of fluorescence imaging and should greatly benefit systematic biology investigations.

Two sets of highly sensitive and multiplexed Raman palettes have been developed for SRS imaging over the past five years. The first is xanthene-based electronic preresonance enhanced Manhattan Raman scattering (MARS) dyes[47,48] (Figure 6a). By careful tuning of the absorption of the dyes (650−760 nm) to moderately close to the laser wavelength (~900 nm), SRS intensities of the nitrile vibration from these dyes could be preresonantly enhanced by up to 10^4 folds (detection limit down to 250 nM) with a well-maintained high signal-to-background ratio (Figure 6b,c). Taking advantage of the much narrower (78 times, 13 vs 1020 cm^{-1} of fwhm) SRS peak compared with the fluorescence absorption peak and multiplexing from isotope labeling as illustrated in the example of MARS2228 series dyes (Figure 6c), MARS dyes have an inherent capability for super-multiplexed imaging. With central atom (position 10) replacement, ring expansion, and isotope editing, an SRS dye palette with up to 24-plex signaling was

https://doi.org/10.1021/acschembio.2c00200
ACS Chem. Biol. 2022, 17, 1621−1637

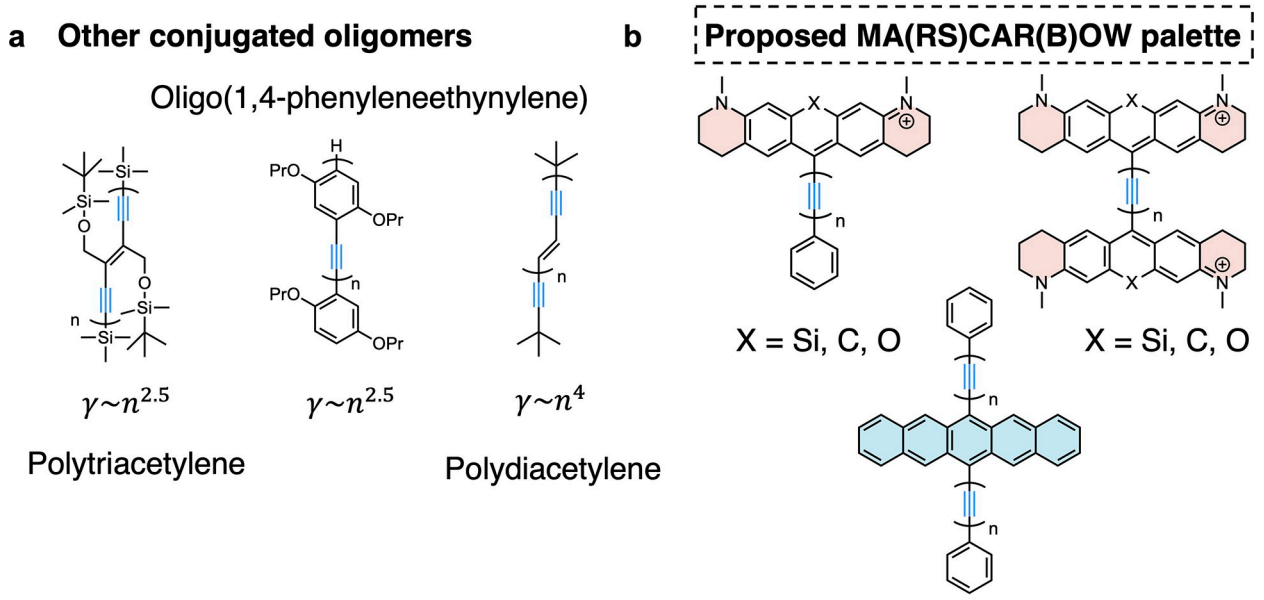

Figure 7. Possible oligomers and proposed MA(RS)CAR(B)OW palette as next-generation strong Raman probes. (a) Other alkyne-conjugated oligomers with a similar exponential power-law relationship between the second-order hyperpolarizability (γ) and repeating units (n). (b) Molecule designs for building stronger Raman probes by simultaneously utilizing the electronic preresonance and hyperpolarizability enhancing effects.

created for super-multiplexed imaging[47] (Figure 6d). Through investigations in our lab, we later found that different scaffolds could present vastly different preresonance SRS signals even with the same absorption wavelength, possibly due to the complicated electronic−vibrational coupling strength. This indicates that finding the right chemical scaffold is as important as physically modulating the absorption of the electronic structures. To facilitate the development of new palettes, theoretical models and computational tools are also urgently needed.[101] While the construction of near-infrared chromophores is more challenging, the suitable electronic preresonance palettes could be largely expanded when freely tunable laser sources in the visible range are available.[102,103]

The second established set of highly sensitive Raman probes is the Carbow series, which is a set of linear conjugated alkynes with aromatic capping[104] (Figure 6e). Different from the electronic enhancement mechanism, the strong SRS signals of polyynes originate from the amplified second-order hyperpolarizability (γ) from conjugated alkynes. When the number of conjugated alkynes increases from 2 to 6, the Raman intensity grows superlinearly with an exponent of 2.77 (i.e., $\gamma \approx n^{2.77}$, Figure 6f), offering a desirable detectability down to 630 nM for 4-yne. The increase of conjugation length is also accompanied by a desirable Raman peak shift, offering more spectral resolvability for multiplexed applications. Further combined with end-capping substitution and isotope editing, another 20-color Carbow palette was created (Figure 6g). Without the involvement of electronic excitation, polyynes are free of photobleaching or environmental quenching. Although slightly smaller in Raman cross section compared to the MARS palette, the Carbow palette has neutral scaffolds and is more suitable for live-cell targeted imaging with lower nonspecific background. Theoretically, the longest conjugation length of polyynes could be over 6 with higher sensitivity than MARS but at the risk of decreased stability. Going beyond the polyyne structures, other oligomers, such as polytriacetylenes, oligo(1,4-phenylene ethynylene)s,[105] and polydiacetylenes,[77] have also shown an exponential power-law relationship between the second-order hyperpolarizability (γ) and repeating units (n) with slightly increased sizes (Figure 7a)[106] and thus are promising candidates for next-generation strong Raman probes.

The ultimate goal of improving the signals of Raman probes is to achieve single-molecule SRS imaging, meaning that even for the most sensitive MARS probes, a sensitivity improvement of ∼30−50-fold is still needed. Toward this goal, a possible design direction for Raman probes is to combine MARS and Carbow scaffolds in the same molecules for cooperative enhancement from electronic preresonance and the amplified γ (Figure 7b), that is, to replace the single alkyne in the current alkyne-containing MARS probes with conjugated polyynes (Figure 7b). In the case that the preresonance effect remains, the Raman signal is also expected to undergo an exponential increase with the number of conjugated alkynes, thus the resulting MA(RS)CAR(B)OW palette might have dozens of times additional enhancement compared with the MARS palette to meet the desired single-molecule detectability.

FUNCTIONAL RAMAN IMAGING PROBES

Probing biological systems through chemical probes is a central topic for chemical biology study. Leveraging the live-cell compatibility, strict linear-concentration dependence, and nonquenching nature of Raman signals, SRS probes are preferred for quantitative analysis. Although small vibrational probes have been extensively utilized for spectroscopic analysis of the targeted cellular environment, such as electrostatic interactions, electrical currents, and temperature,[4,62,63] the development of highly sensitive Raman imaging probes for environmental sensing is still in its infancy. Benefiting from the unique super-multiplexed Raman features, functional SRS imaging probes should open the door for comprehensive investigations to elucidate intricate intracellular and cell-to-cell interactions. Over the past four years, we witnessed the rapid growth of the development of such highly sensitive SRS sensors. Based on their Raman spectroscopic features, we categorized these Raman sensors into four classes: sensing by

https://doi.org/10.1021/acschembio.2c00200
ACS Chem. Biol. 2022, 17, 1621−1637

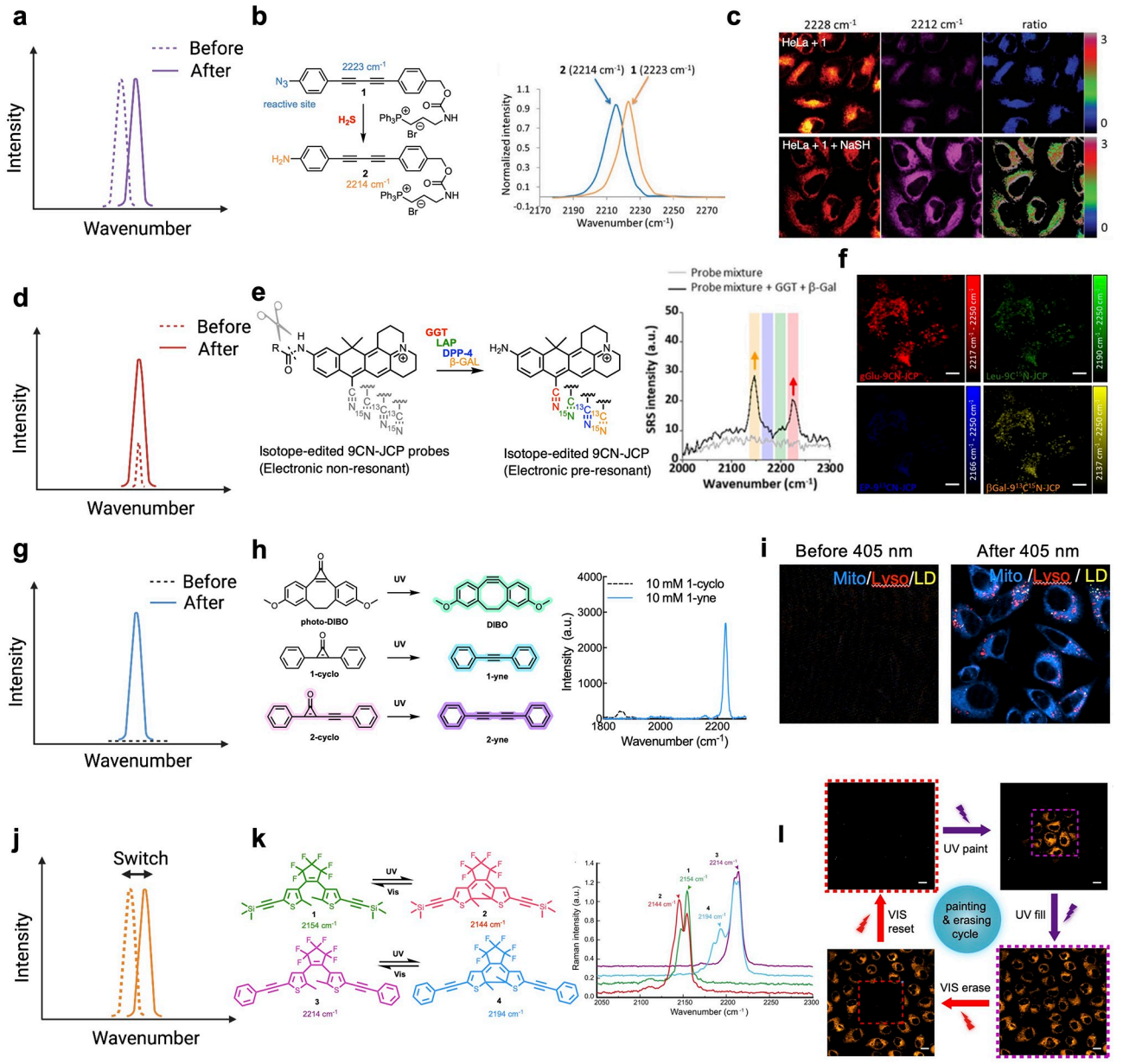

Figure 8. SRS probes for functional imaging with different spectroscopic signatures and their chemical designs. (a) SRS sensors based on peak shifts. (b) Conversion of $—N_3$ to $—NH_2$ induces a Raman peak shift of 9 cm^{-1} on the core of 2-yne. Adapted in part with permission from ref 107. Copyright 2018 The Royal Society of Chemistry. (c) Ratiometric imaging for NaSH sensing from the peak shift of the probe **1**. Adapted in part with permission from ref 107. Copyright 2018 The Royal Society of Chemistry. (d) SRS sensors based on peak enhancements. (e) Electronic nonresonant 9CN-JCP probes undergo a large enzyme-induced red shift in absorption to the electronic preresonant region with dramatic enhancement of SRS signals. Adapted in part with permission from ref 50. Copyright 2020 American Chemical Society. (f) Enhanced SRS signals enable multiplexed imaging for live-cell enzyme (GGT, LAP, DPP-4, and β-Gal) sensing. Scale bars 10 μm. Adapted in part with permission from ref 50. Copyright 2020 American Chemical Society. (g) SRS sensors based on the peak generation. (h) Photoreactive conversion of cyclopropenones into alkynes generates strong SRS contrast with a sharp Raman peak. Adapted in part with permission from ref 54. Copyright 2022 American Chemical Society. (i) Engineered cyclopropenone probes enable three-color organelle-target photoactivatable SRS imaging in live HeLa cells (Mito, mitochondria channel; Lyso, lysosome channel; LD, lipid droplet channel). Adapted in part with permission from ref 54. Copyright 2022 American Chemical Society. (j) SRS sensors based on switchable peaks. (k) Raman peak shifts reversibly upon photoisomerization of the diarylethene when irradiated by ultraviolet (UV) or visible light. Adapted in part with permission from ref 51. Copyright 2021 Nature Publishing Group. (l) This photoswitchable peak shift enables SRS painting/erasing of cells with labeled alkyne−diarylethene. Scale bars 20 μm. Adapted in part with permission from ref 51. Copyright 2021 Nature Publishing Group.

peak shifts, peak enhancement, peak generation, and peak switching. Through the following discussions, we aim to summarize systematic guidelines for designing new probes with tailored functions.

Most current Raman sensors are designed for sensing the targeted chemical environment through Raman peak shifts (Figure 8a). The chemical reactions triggered by environmental stimuli are designed to change the chemical structures adjacent to the Raman reporters (e.g., alkynes or nitriles), therefore resulting in distinct Raman peak shifts. For example, in a 2-yne scaffold, when the electron-withdrawing azide group on the end phenyl cap is reduced to the electron-donating

https://doi.org/10.1021/acschembio.2c00200
ACS Chem. Biol. 2022, 17, 1621−1637

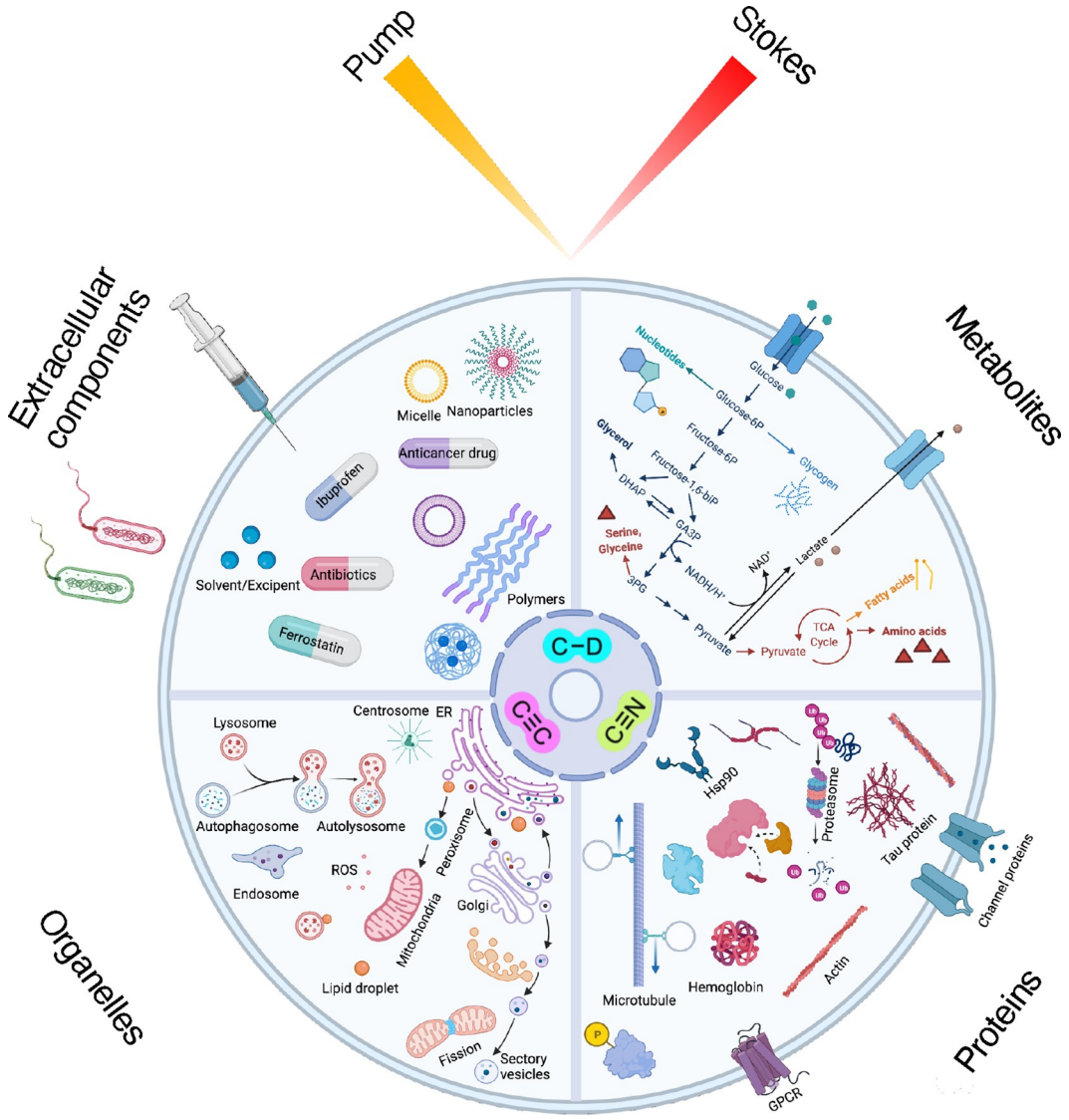

Figure 9. Representative and envisioned applications of SRS imaging, particularly with the development of Raman-tailored bioorthogonal chemical tags of C≡C, C≡N, and C—D. The dynamic processes of targets across different molecular scales, from small-molecule metabolites to proteins, organelles, and extracellular components, can be visualized with high specificity and low perturbation.

amine in the presence of a reductive hydrogen sulfide species (such as H_2S and NaSH), the alkyne Raman peak shows a 9 cm^{-1} red shift[107] (Figure 8b), which is significant enough to be distinguished by SRS imaging (the typical full width at half-maximum (fwhm) for an alkyne peak is 15 cm^{-1} and the typical spectral width of SRS lasers is ∼12−15 cm^{-1}). The demonstrated SRS ratiometric imaging indeed showed a strong response to NaSH level changes in the mitochondria of live cells (Figure 8c). With similar targeted reactions, triple-bond Raman probes with the peak-shift principles have also been rationally designed and developed for sensing pH,[108] fluoride,[109] and metal ions.[110] Recently, the isotope exchange reactions (especially the H/D exchange) have been harnessed on the terminal alkynes for both two-color imaging and cellular environmental sensing applications.[111,112] The H/D exchange reaction results in the dramatic alkyne Raman peak shift (>130 cm^{-1}) due to both the large mass difference between D and H and the quantum coupling between the alkyne and the adjacent C—D. In addition to chemical reactions, Raman peak frequency can also be tuned by the surrounding physical environment. A well-known example is that hydrogen-bounding and electrostatics can shift the peak frequencies of triple bonds, especially nitriles, an effect known as vibrational solvatochromism. By specifically mapping the peak frequency of a nitrile-bearing MARS Raman dye in live cells, the bound-water percentage in cytoplasm was revealed to be around 60%, while that in nucleus was about 30%.[113,114] Recently, the SRS peak of voltage-sensitive rhodopsin has also been shown to shift upon voltage changes.[115]

Intensity enhancement represents another less explored category of design principles for SRS sensors (Figure 8d). Recently, modulation of electronic preresonance SRS effect was implemented for intracellular enzyme activity sensing. The nitrile xanthene scaffold, once caged by amide structures (9CN-JCP probes), will absorb in the visible region (506 nm, electronic nonresonance) with almost invisible SRS signals. However, the enzymatic conversion of amide structures to amine structures (9CN-JCPs) will dramatically boost SRS signals by shifting the absorption to the near-infrared region (630 nm, electronic preresonance) (Figure 8e). With isotope

https://doi.org/10.1021/acschembio.2c00200
ACS Chem. Biol. 2022, 17, 1621−1637

editing on the nitrile to generate multiple colors, this elegant intensity-modulation principle was successfully exploited to create a 4-color enzymatic sensing probe palette[50] (Figure 8e). In this case, simultaneously detecting the activities of four distinct enzymes was demonstrated for effective profiling of different cancer cell phenotypes (Figure 8f). With the super-multiplexed MARS dye palette, this enzyme-activatable sensor design holds high promise for profiling more than ten enzymes simultaneously.

Peak generation allows background-free imaging and is highly beneficial for sensitive and multiplexed detection (Figure 8g). The Raman intensity activation can not only come from the cellular or the chemical environment, but also originate from the photons. In a recent design, the first photoactivatable SRS imaging probes were developed based on photocaged alkynes, the cyclopropenones (Figure 8h).[54] Such rationally designed cyclopropenone structures were optimized with live-cell compatibility and have been proven to be highly suitable for multiplexed live-cell imaging and tracking[54] (Figure 8i). With the high precision spatial-temporal control offered by photoactivation, this series of isotope editing probes was demonstrated for multiplexed tracking from the subcellular to the single-cell level. Upon further improvement of multiplexing, these new Raman sensors may illuminate complex cell-to-cell interactions and facilitate massively parallel cell profiling. For example, combining photoactivatable SRS probes and single-cell RNA sequencing (scRNA-seq) could likely enable spatially resolved transcriptomics profiling.[116]

Raman peaks could also be reversibly switchable with light manipulation (Figure 8j). Such features are crucial to a variety of biological investigations including tracking protein dynamics, sensing subcellular environments and imaging ultrastructures beyond the diffraction limit. In 2021, three groups independently reported photophysical or photochemical approaches to achieve photoswitchable SRS imaging.[51−53] To name one example, the alkyne-tagged diarylethene showed impressive photoswitchable properties in the cell-silent spectral window[51] (Figure 8k). The UV induced photoisomerization converts diarylethene from the open-ring state to the closed-ring state, while visible light induces the reverse conversion, accompanied by the switching of SRS peak intensities. These alkyne-tagged diarylethenes were demonstrated for photo-rewritable patterning and mitochondrial tracking (Figure 8l). It is noteworthy that the SRS readout lasers would induce the off-switch pathway, competing with the UV induced photocyclization, underscoring the careful choice of molecular absorption when designing the new probes.

CONCLUSION

Through the past decade, we have seen that the SRS microscopy has transitioned from the initial technical demonstration into a powerful method with the potential to answer many biological questions in a way that no other methods can (Figure 9). Such transformation is impossible without appropriate Raman probes. With small triple-bond or isotope tagging, SRS microscopy enables the visualization and analysis of dynamic metabolism pathways in live cells and animals. From chemical innovations, the construction of highly sensitive MARS and Carbow palettes realized the full potential of Raman for super-multiplexed imaging. Recently developed functional Raman sensors have further expanded the applications for multiplexed cellular environment sensing and high precision spatial-temporal tracking. We also envision designs with further improved multiplexing and sensitivity of the Raman probes as a next step toward interrogating more complex biology.

As the development of Raman probes continues to be a central topic for the SRS community, we also hope to invoke brainstorming to borrow wisdom from the chemical biology field and to promote vibrational imaging to solve biological questions. In retrospect, much of the recent progress on SRS probes was inspired by other fields: labeling with deuterium and other isotopes is prevalent in mass spectrometry; alkynes are the most important biorthogonal chemical group handles; MARS dyes originate from the design of commercially available fluorophores; diarylethene represents a class of well-established photoswitchable chromophores, etc. The knowledge across fields should accelerate the advances of SRS probes into higher selectivity, sensitivity, photostability, biocompatibility, and multiplexing capability. Together with the developments of instrumentation, biorthogonal chemistry, molecular delivery and labeling methods, data analysis, and more, SRS microscopy will further develop into an indispensable tool for chemical biology studies.

AUTHOR INFORMATION

Corresponding Author

Lu Wei − *Division of Chemistry and Chemical Engineering, California Institute of Technology, Pasadena, California 91125, United States;* orcid.org/0000-0001-9170-2283; Email: lwei@caltech.edu

Authors

Jiajun Du − *Division of Chemistry and Chemical Engineering, California Institute of Technology, Pasadena, California 91125, United States;* orcid.org/0000-0003-2693-834X

Haomin Wang − *Division of Chemistry and Chemical Engineering, California Institute of Technology, Pasadena, California 91125, United States*

Complete contact information is available at: https://pubs.acs.org/10.1021/acschembio.2c00200

Notes

The authors declare no competing financial interest.

ACKNOWLEDGMENTS

L. Wei acknowledges startup funds from California Institute of Technology and Grant No. DP2 GM140919 from the National Institutes of Health. We thank A. Colazo for helpful discussion.

REFERENCES

(1) Kneipp, K.; Kneipp, H.; Itzkan, I.; Dasari, R. R.; Feld, M. S. Ultrasensitive Chemical Analysis by Raman Spectroscopy. *Chem. Rev.* **1999**, *99* (10), 2957−2975.

(2) Fang, C.; Frontiera, R. R.; Tran, R.; Mathies, R. A. Mapping GFP Structure Evolution during Proton Transfer with Femtosecond Raman Spectroscopy. *Nature* **2009**, *462* (7270), 200−204.

(3) Kukura, P.; McCamant, D. W.; Mathies, R. A. Femtosecond Stimulated Raman Spectroscopy. *Annu. Rev. Phys. Chem.* **2007**, *58*, 461−488.

(4) Chattopadhyay, A.; Boxer, S. G. Vibrational Stark Effect Spectroscopy. *J. Am. Chem. Soc.* **1995**, *117* (4), 1449−1450.

(5) Thomas, G. J. Raman Spectroscopy of Protein and Nucleic Acid Assemblies. *Annu. Rev. Biophys. Biomol. Struct.* **1999**, *28*, 1−27.

(6) Raman, C. V.; Krishnan, K. S. A New Type of Secondary Radiation [11]. *Nature* **1928**, *121* (3048), 501−502.

(7) Zumbusch, A.; Holtom, G. R.; Xie, X. S. Three-Dimensional Vibrational Imaging by Coherent Anti-Stokes Raman Scattering. *Phys. Rev. Lett.* **1999**, *82* (20), 4142−4145.
(8) Min, W.; Freudiger, C. W.; Lu, S.; Xie, X. S. Coherent Nonlinear Optical Imaging: Beyond Fluorescence Microscopy. *Annu. Rev. Phys. Chem.* **2011**, *62*, 507−530.
(9) Ploetz, E.; Laimgruber, S.; Berner, S.; Zinth, W.; Gilch, P. Femtosecond Stimulated Raman Microscopy. *Appl. Phys. B Lasers Opt.* **2007**, *87* (3), 389−393.
(10) Freudiger, C. W.; Min, W.; Saar, B. G.; Lu, S.; Holtom, G. R.; He, C.; Tsai, J. C.; Kang, J. X.; Xie, S. Label-Free Biomedical Imaging with High Sensitivity by Stimulated Raman Scattering Microscopy. *Science* **2008**, *322* (19), 1857−1861.
(11) Ozeki, Y.; Dake, F.; Kajiyama, S.; Fukui, K.; Itoh, K. Analysis and Experimental Assessment of the Sensitivity of Stimulated Raman Scattering Microscopy. *Opt. Express* **2009**, *17* (5), 3651.
(12) Cheng, J. X.; Xie, X. S. Vibrational Spectroscopic Imaging of Living Systems: An Emerging Platform for Biology and Medicine. *Science* **2015**, *350* (6264), aaa8870.
(13) Hu, F.; Shi, L.; Min, W. Biological Imaging of Chemical Bonds by Stimulated Raman Scattering Microscopy. *Nat. Methods* **2019**, *16* (9), 830−842.
(14) Saar, B. G.; Freudiger, C. W.; Reichman, J.; Stanley, C. M.; Holtom, G. R.; Xie, X. S. Video-Rate Molecular Imaging in Vivo with Stimulated Raman Scattering. *Science* **2010**, *330* (6009), 1368−1370.
(15) Camp, C. H.; Lee, Y. J.; Heddleston, J. M.; Hartshorn, C. M.; Walker, A. R. H.; Rich, J. N.; Lathia, J. D.; Cicerone, M. T. High-Speed Coherent Raman Fingerprint Imaging of Biological Tissues. *Nat. Photonics* **2014**, *8* (8), 627−634.
(16) Wakisaka, Y.; Suzuki, Y.; Iwata, O.; Nakashima, A.; Ito, T.; Hirose, M.; Domon, R.; Sugawara, M.; Tsumura, N.; Watarai, H. Probing the Metabolic Heterogeneity of Live Euglena Gracilis with Stimulated Raman Scattering Microscopy. *Nat. Microbiol.* **2016**, *1*, No. 16124.
(17) Bi, Y.; Yang, C.; Chen, Y.; Yan, S.; Yang, G.; Wu, Y.; Zhang, G.; Wang, P. Near-Resonance Enhanced Label-Free Stimulated Raman Scattering Microscopy with Spatial Resolution near 130 Nm. *Light Sci. Appl.* **2018**, *7* (1), 1−10.
(18) Qian, C.; Miao, K.; Lin, L. E.; Chen, X.; Du, J.; Wei, L. Super-Resolution Label-Free Volumetric Vibrational Imaging. *Nat. Commun.* **2021**, *12* (1), 1−10.
(19) Shi, L.; Klimas, A.; Gallagher, B.; Cheng, Z.; Fu, F.; Wijesekara, P.; Miao, Y.; Ren, X.; Zhao, Y.; Min, W. Super-Resolution Vibrational Imaging Using Expansion Stimulated Raman Scattering Microscopy. *Adv. Sci.* **2022**, 2200315.
(20) Zipfel, W. R.; Williams, R. M.; Webb, W. W. Nonlinear Magic: Multiphoton Microscopy in the Biosciences. *Nat. Biotechnol.* **2003**, *21* (11), 1369−1377.
(21) Jonkman, J.; Brown, C. M.; Wright, G. D.; Anderson, K. I.; North, A. J. Tutorial: Guidance for Quantitative Confocal Microscopy. *Nat. Protoc.* **2020**, *15* (5), 1585−1611.
(22) Miller, D. R.; Jarrett, J. W.; Hassan, A. M.; Dunn, A. K. Deep Tissue Imaging with Multiphoton Fluorescence Microscopy. *Curr. Opin. Biomed. Eng.* **2017**, *4*, 32−39.
(23) Hill, A. H.; Manifold, B.; Fu, D. Tissue Imaging Depth Limit of Stimulated Raman Scattering Microscopy. *Biomed. Opt. Express* **2020**, *11* (2), 762.
(24) Fu, D.; Holtom, G.; Freudiger, C.; Zhang, X.; Xie, X. S. Hyperspectral Imaging with Stimulated Raman Scattering by Chirped Femtosecond Lasers. *J. Phys. Chem. B* **2013**, *117* (16), 4634−4640.
(25) Zhang, D.; Wang, P.; Slipchenko, M. N.; Ben-Amotz, D.; Weiner, A. M.; Cheng, J. X. Quantitative Vibrational Imaging by Hyperspectral Stimulated Raman Scattering Microscopy and Multivariate Curve Resolution Analysis. *Anal. Chem.* **2013**, *85* (1), 98−106.
(26) Figueroa, B.; Hu, R.; Rayner, S. G.; Zheng, Y.; Fu, D. Real-Time Microscale Temperature Imaging by Stimulated Raman Scattering. *J. Phys. Chem. Lett.* **2020**, *11* (17), 7083−7089.
(27) Yue, S.; Li, J.; Lee, S.-Y.; Lee, H. J.; Shao, T.; Song, B.; Cheng, L.; Masterson, T. A.; Liu, X.; Ratliff, T. L.; et al. Cholesteryl Ester Accumulation Induced by PTEN Loss and PI3KAKT Activation Underlies Human Prostate Cancer Aggressiveness. *Cell Metab.* **2014**, *19*, 393−406.
(28) Li, J.; Condello, S.; Thomes-Pepin, J.; Ma, X.; Xia, Y.; Hurley, T. D.; Matei, D.; Cheng, J. X. Lipid Desaturation Is a Metabolic Marker and Therapeutic Target of Ovarian Cancer Stem Cells. *Cell Stem Cell* **2017**, *20* (3), 303−314.
(29) Du, J.; Su, Y.; Qian, C.; Yuan, D.; Miao, K.; Lee, D.; Ng, A. H. C.; Wijker, R. S.; Ribas, A.; Levine, R. D.; et al. Raman-Guided Subcellular Pharmaco-Metabolomics for Metastatic Melanoma Cells. *Nat. Commun.* **2020**, *11* (1), 4830.
(30) Chen, T.; Yavuz, A.; Wang, M. C. Dissecting Lipid Droplet Biology with Coherent Raman Scattering Microscopy. *J. Cell Sci.* **2022**, *135* (5), No. jcs252353.
(31) Shen, Y.; Zhao, Z.; Zhang, L.; Shi, L.; Shahriar, S.; Chan, R. B.; Di Paolo, G.; Min, W. Metabolic Activity Induces Membrane Phase Separation in Endoplasmic Reticulum. *Proc. Natl. Acad. Sci. U. S. A.* **2017**, *114* (51), 13394−13399.
(32) Wei, L.; Hu, F.; Shen, Y.; Chen, Z.; Yu, Y.; Lin, C. C.; Wang, M. C.; Min, W. Live-Cell Imaging of Alkyne-Tagged Small Biomolecules by Stimulated Raman Scattering. *Nat. Methods* **2014**, *11* (4), 410−412.
(33) Chiu, W. S.; Belsey, N. A.; Garrett, N. L.; Moger, J.; Delgado-Charro, M. B.; Guy, R. H. Molecular Diffusion in the Human Nail Measured by Stimulated Raman Scattering Microscopy. *Proc. Natl. Acad. Sci. U. S. A.* **2015**, *112* (25), 7725−7730.
(34) Fu, D.; Zhou, J.; Zhu, W. S.; Manley, P. W.; Wang, Y. K.; Hood, T.; Wylie, A.; Xie, X. S. Imaging the Intracellular Distribution of Tyrosine Kinase Inhibitors in Living Cells with Quantitative Hyperspectral Stimulated Raman Scattering. *Nat. Chem.* **2014**, *6* (7), 614−622.
(35) Huang, K. C.; Li, J.; Zhang, C.; Tan, Y.; Cheng, J. X. Multiplex Stimulated Raman Scattering Imaging Cytometry Reveals Lipid-Rich Protrusions in Cancer Cells under Stress Condition. *iScience* **2020**, *23* (3), 100953.
(36) Nitta, N.; Iino, T.; Isozaki, A.; Yamagishi, M.; Kitahama, Y.; Sakuma, S.; Suzuki, Y.; Tezuka, H.; Oikawa, M.; Arai, F.; et al. Raman Image-Activated Cell Sorting. *Nat. Commun.* **2020**, *11* (1), 1−16.
(37) Ji, M.; Orringer, D. A.; Freudiger, C. W.; Ramkissoon, S.; Liu, X.; Lau, D.; Golby, A. J.; Norton, I.; Hayashi, M.; Agar, N. Y. R. Rapid, Label-Free Detection of Brain Tumors with Stimulated Raman Scattering Microscopy. *Sci. Transl. Med.* **2013**, *5* (201), No. 201ra119.
(38) Hollon, T. C.; Pandian, B.; Adapa, A. R.; Urias, E.; Save, A. V.; Khalsa, S. S. S.; Eichberg, D. G.; D'Amico, R. S.; Farooq, Z. U.; Lewis, S.; et al. Near Real-Time Intraoperative Brain Tumor Diagnosis Using Stimulated Raman Histology and Deep Neural Networks. *Nat. Med.* **2020**, *26* (1), 52−58.
(39) Ji, M.; Arbel, M.; Zhang, L.; Freudiger, C. W.; Hou, S. S.; Lin, D.; Yang, X.; Bacskai, B. J.; Xie, X. S. Label-Free Imaging of Amyloid Plaques in Alzheimer's Disease with Stimulated Raman Scattering Microscopy. *Sci. Adv.* **2018**, *4* (11), eaat7715.
(40) Lin, L. E.; Miao, K.; Qian, C.; Wei, L. High Spatial-Resolution Imaging of Label-Free in Vivo Protein Aggregates by VISTA. *Analyst* **2021**, *146* (13), 4135−4145.
(41) Berto, P.; Andresen, E. R.; Rigneault, H. Background-Free Stimulated Raman Spectroscopy and Microscopy. *Phys. Rev. Lett.* **2014**, *112* (5), 1−5.
(42) Casacio, C. A.; Madsen, L. S.; Terrasson, A.; Waleed, M.; Barnscheidt, K.; Hage, B.; Taylor, M. A.; Bowen, W. P. Quantum-Enhanced Nonlinear Microscopy. *Nature* **2021**, *594* (7862), 201−206.
(43) Lin, H.; Lee, H. J.; Tague, N.; Lugagne, J.-B.; Zong, C.; Deng, F.; Shin, J.; Tian, L.; Wong, W.; Dunlop, M. J.; Cheng, J.-X. Microsecond Fingerprint Stimulated Raman Spectroscopic Imaging by Ultrafast Tuning and Spatial-Spectral Learning. *Nat. Commun.* **2021**, *12* (1), 3052.
(44) Kobayashi-Kirschvink, K. J.; Gaddam, S.; James-Sorenson, T.; Grody, E.; Ounadjela, J. R.; Ge, B.; Zhang, K.; Kang, J. W.; Xavier, R.; So, P. T. C.; et al. Raman2RNA: Live-Cell Label-Free Prediction of

https://doi.org/10.1021/acschembio.2c00200
ACS Chem. Biol. 2022, 17, 1621−1637

Single-Cell RNA Expression Profiles by Raman Microscopy. *bioRxiv* **2021**, DOI: 10.1101/2021.11.30.470655.
(45) Manifold, B.; Men, S.; Hu, R.; Fu, D. A Versatile Deep Learning Architecture for Classification and Label-Free Prediction of Hyperspectral Images. *Nat. Mach. Intell.* **2021**, *3* (4), 306−315.
(46) Wei, L.; Hu, F.; Chen, Z.; Shen, Y.; Zhang, L.; Min, W. Live-Cell Bioorthogonal Chemical Imaging: Stimulated Raman Scattering Microscopy of Vibrational Probes. *Acc. Chem. Res.* **2016**, *49* (8), 1494−1502.
(47) Wei, L.; Chen, Z.; Shi, L.; Long, R.; Anzalone, A. V.; Zhang, L.; Hu, F.; Yuste, R.; Cornish, V. W.; Min, W. Super-Multiplex Vibrational Imaging. *Nature* **2017**, *544*, 465.
(48) Miao, Y.; Qian, N.; Shi, L.; Hu, F.; Min, W. 9-Cyanopyronin Probe Palette for Super-Multiplexed Vibrational Imaging. *Nat. Commun.* **2021**, *12*, 4518.
(49) Shi, L.; Wei, M.; Miao, Y.; Qian, N.; Shi, L.; Singer, R. A.; Benninger, R. K. P.; Min, W. Highly-Multiplexed Volumetric Mapping with Raman Dye Imaging and Tissue Clearing. *Nat. Biotechnol.* **2022**, *40*, 364.
(50) Fujioka, H.; Shou, J.; Kojima, R.; Urano, Y.; Ozeki, Y.; Kamiya, M. Multicolor Activatable Raman Probes for Simultaneous Detection of Plural Enzyme Activities. *J. Am. Chem. Soc.* **2020**, *142* (49), 20701−20707.
(51) Ao, J.; Fang, X.; Miao, X.; Ling, J.; Kang, H.; Park, S.; Wu, C.; Ji, M. Switchable Stimulated Raman Scattering Microscopy with Photochromic Vibrational Probes. *Nat. Commun.* **2021**, *12* (1), 1−8.
(52) Shou, J.; Ozeki, Y. Photoswitchable Stimulated Raman Scattering Spectroscopy and Microscopy. *Opt. Lett.* **2021**, *46* (9), 2176.
(53) Lee, D.; Qian, C.; Wang, H.; Li, L.; Miao, K.; Du, J.; Shcherbakova, D. M.; Verkhusha, V. V.; Wang, L. V.; Wei, L. Toward Photoswitchable Electronic Pre-Resonance Stimulated Raman Probes. *J. Chem. Phys.* **2021**, *154*, 135102.
(54) Du, J.; Wei, L. Multicolor Photoactivatable Raman Probes for Subcellular Imaging and Tracking by Cyclopropenone Caging. *J. Am. Chem. Soc.* **2022**, *144*, 777.
(55) Hong, S.; Chen, T.; Zhu, Y.; Li, A.; Huang, Y.; Chen, X. Live-Cell Stimulated Raman Scattering Imaging of Alkyne-Tagged Biomolecules. *Angew. Chemie - Int. Ed.* **2014**, *53* (23), 5827−5831.
(56) Lee, H. J.; Zhang, W.; Zhang, D.; Yang, Y.; Liu, B.; Barker, E. L.; Buhman, K. K.; Slipchenko, L. V.; Dai, M.; Cheng, J. X. Assessing Cholesterol Storage in Live Cells and C. Elegans by Stimulated Raman Scattering Imaging of Phenyl-Diyne Cholesterol. *Sci. Rep.* **2015**, *5*, 7930.
(57) de Moliner, F.; Knox, K.; Gordon, D.; Lee, M.; Tipping, W. J.; Geddis, A.; Reinders, A.; Ward, J. M.; Oparka, K.; Vendrell, M. A Palette of Minimally Tagged Sucrose Analogues for Real-Time Raman Imaging of Intracellular Plant Metabolism. *Angew. Chemie - Int. Ed.* **2021**, *60* (14), 7637−7642.
(58) Seidel, J.; Miao, Y.; Porterfield, W.; Cai, W.; Zhu, X.; Kim, S. J.; Hu, F.; Bhattarai-Kline, S.; Min, W.; Zhang, W. Structure-Activity-Distribution Relationship Study of Anti-Cancer Antimycin-Type Depsipeptides. *Chem. Commun.* **2019**, *55* (63), 9379−9382.
(59) Gaschler, M. M.; Hu, F.; Feng, H.; Linkermann, A.; Min, W.; Stockwell, B. R. Determination of the Subcellular Localization and Mechanism of Action of Ferrostatins in Suppressing Ferroptosis. *ACS Chem. Biol.* **2018**, *13* (4), 1013−1020.
(60) Koike, K.; Bando, K.; Ando, J.; Yamakoshi, H.; Terayama, N.; Dodo, K.; Smith, N. I.; Sodeoka, M.; Fujita, K. Quantitative Drug Dynamics Visualized by Alkyne-Tagged Plasmonic-Enhanced Raman Microscopy. *ACS Nano* **2020**, *14* (11), 15032−15041.
(61) Chen, Z.; Paley, D. W.; Wei, L.; Weisman, A. L.; Friesner, R. A.; Nuckolls, C.; Min, W. Multicolor Live-Cell Chemical Imaging by Isotopically Edited Alkyne Vibrational Palette. *J. Am. Chem. Soc.* **2014**, *136* (22), 8027−8033.
(62) Waegele, M. M.; Culik, R. M.; Gai, F. Site-Specific Spectroscopic Reporters of the Local Electric Field, Hydration, Structure, and Dynamics of Biomolecules. *J. Phys. Chem. Lett.* **2011**, *2* (20), 2598−2609.
(63) Bakthavatsalam, S.; Dodo, K.; Sodeoka, M. A Decade of Alkyne-Tag Raman Imaging (ATRI): Applications in Biological Systems. *RSC Chem. Biol.* **2021**, *2*, 1415−1429.
(64) Yamakoshi, H.; Dodo, K.; Palonpon, A.; Ando, J.; Fujita, K.; Kawata, S.; Sodeoka, M. Alkyne-Tag Raman Imaging for Visualization of Mobile Small Molecules in Live Cells. *J. Am. Chem. Soc.* **2012**, *134* (51), 20681−20689.
(65) Hu, F.; Chen, Z.; Zhang, L.; Shen, Y.; Wei, L.; Min, W. Vibrational Imaging of Glucose Uptake Activity in Live Cells and Tissues by Stimulated Raman Scattering. *Angew. Chem., Int. Ed.* **2015**, *54* (34), 9821−9825.
(66) Wei, L.; Yu, Y.; Shen, Y.; Wang, M. C.; Min, W. Vibrational Imaging of Newly Synthesized Proteins in Live Cells by Stimulated Raman Scattering Microscopy. *Proc. Natl. Acad. Sci. U. S. A.* **2013**, *110* (28), 11226−11231.
(67) Saar, B. G.; Contreras-Rojas, L. R.; Xie, S. X.; Guy, R. H. Imaging Drug Delivery to Skin with Coherent Raman Scattering Microscopy. *Mol. Pharmaceutics* **2011**, *8*, 969−975.
(68) Miao, K.; Wei, L. Live-Cell Imaging and Quantification of PolyQ Aggregates by Stimulated Raman Scattering of Selective Deuterium Labeling. *ACS Cent. Sci.* **2020**, *6* (4), 478−486.
(69) Hu, F.; Brucks, S. D.; Lambert, T. H.; Campos, L. M.; Min, W. Stimulated Raman Scattering of Polymer Nanoparticles for Multiplexed Live-Cell Imaging. *Chem. Commun.* **2017**, *53* (46), 6187−6190.
(70) Li, J.; Cheng, J. X. Direct Visualization of de Novo Lipogenesis in Single Living Cells. *Sci. Rep.* **2015**, *4*, 6807.
(71) Zhang, D.; Slipchenko, M. N.; Cheng, J. X. Highly Sensitive Vibrational Imaging by Femtosecond Pulse Stimulated Raman Loss. *J. Phys. Chem. Lett.* **2011**, *2* (11), 1248−1253.
(72) Hu, F.; Wei, L.; Zheng, C.; Shen, Y.; Min, W. Live-Cell Vibrational Imaging of Choline Metabolites by Stimulated Raman Scattering Coupled with Isotope-Based Metabolic Labeling. *Analyst* **2014**, *139* (10), 2312−2317.
(73) Alfonso-García, A.; Pfisterer, S. G.; Riezman, H.; Ikonen, E.; Potma, E. O. D38-Cholesterol as a Raman Active Probe for Imaging Intracellular Cholesterol Storage. *J. Biomed. Opt.* **2016**, *21* (6), 061003.
(74) Shi, L.; Zheng, C.; Shen, Y.; Chen, Z.; Silveira, E. S.; Zhang, L.; Wei, M.; Liu, C.; de Sena-Tomas, C.; Targoff, K.; et al. Optical Imaging of Metabolic Dynamics in Animals. *Nat. Commun.* **2018**, *9* (1), No. 2995, DOI: 10.1038/s41467-018-05401-3.
(75) Lee, D.; Du, J.; Yu, R.; Su, Y.; Heath, J. R.; Wei, L. Visualizing Subcellular Enrichment of Glycogen in Live Cancer Cells by Stimulated Raman Scattering. *Anal. Chem.* **2020**, *92* (19), 13182−13191.
(76) Zhu, W.; Cai, E. L.; Li, H. Z.; Wang, P.; Shen, A. G.; Popp, J.; Hu, J. M. Precise Encoding of Triple-Bond Raman Scattering of Single Polymer Nanoparticles for Multiplexed Imaging Application. *Angew. Chemie - Int. Ed.* **2021**, *60* (40), 21846−21852.
(77) Tian, S.; Li, H.; Li, Z.; Tang, H.; Yin, M.; Chen, Y.; Wang, S.; Gao, Y.; Yang, X.; Meng, F.; et al. Polydiacetylene-Based Ultrastrong Bioorthogonal Raman Probes for Targeted Live-Cell Raman Imaging. *Nat. Commun.* **2020**, *11* (1), 1−9.
(78) Zhao, Z.; Chen, C.; Wei, S.; Xiong, H.; Hu, F.; Miao, Y.; Jin, T.; Min, W. Ultra-Bright Raman Dots for Multiplexed Optical Imaging. *Nat. Commun.* **2021**, *12*, 1305.
(79) Jin, Q. Q.; Fan, X.; Chen, C.; Huang, L.; Wang, J.; Tang, X. Multicolor Raman Beads for Multiplexed Tumor Cell and Tissue Imaging and in Vivo Tumor Spectral Detection. *Anal. Chem.* **2019**, *91* (6), 3784−3789.
(80) Farizyan, M.; Mondal, A.; Mal, S.; Deufel, F.; Van Gemmeren, M. Palladium-Catalyzed Nondirected Late-Stage C-H Deuteration of Arenes. *J. Am. Chem. Soc.* **2021**, *143* (40), 16370−16376.
(81) Zhao, D.; Petzold, R.; Yan, J.; Muri, D.; Ritter, T. Tritiation of Aryl Thianthrenium Salts with a Molecular Palladium Catalyst. *Nature* **2021**, *600* (7889), 444−449.
(82) Porey, S.; Zhang, X.; Bhowmick, S.; Kumar Singh, V.; Guin, S.; Paton, R. S.; Maiti, D. Alkyne Linchpin Strategy for Drug:Pharma-

cophore Conjugation: Experimental and Computational Realization of a Meta-Selective Inverse Sonogashira Coupling. *J. Am. Chem. Soc.* **2020**, *142* (8), 3762−3774.
(83) Yu, Y.; Mutlu, A. S.; Liu, H.; Wang, M. C. High-Throughput Screens Using Photo-Highlighting Discover BMP Signaling in Mitochondrial Lipid Oxidation. *Nat. Commun.* **2017**, *8* (1), 1−11.
(84) Mutlu, A. S.; Gao, S. M.; Zhang, H.; Wang, M. C. Olfactory Specificity Regulates Lipid Metabolism through Neuroendocrine Signaling in Caenorhabditis Elegans. *Nat. Commun.* **2020**, *11* (1), 1−15.
(85) Zhang, L.; Shi, L.; Shen, Y.; Miao, Y.; Wei, M.; Qian, N.; Liu, Y.; Min, W. Spectral Tracing of Deuterium for Imaging Glucose Metabolism. *Nat. Biomed. Eng.* **2019**, *3* (5), 402−413.
(86) Deberardinis, R. J.; Thompson, C. B. Cellular Metabolism and Disease: What Do Metabolic Outliers Teach Us? *Cell* **2012**, *148* (6), 1132−1144.
(87) Long, R.; Zhang, L.; Shi, L.; Shen, Y.; Hu, F.; Zeng, C.; Min, W. Two-Color Vibrational Imaging of Glucose Metabolism Using Stimulated Raman Scattering. *Chem. Commun.* **2018**, *54* (2), 152−155.
(88) Hong, S.; Chen, T.; Liu, L.; Cao, C.; Lv, F.; Rabinowitz, J. D.; Huang, Y.; Chen, X. Live-Cell Imaging of NADPH Production from Specific Pathways. *CCS Chem.* **2021**, *3* (6), 1642−1648.
(89) Zhang, M.; Hong, W.; Abutaleb, N. S.; Li, J.; Dong, P. T.; Zong, C.; Wang, P.; Seleem, M. N.; Cheng, J. X. Rapid Determination of Antimicrobial Susceptibility by Stimulated Raman Scattering Imaging of D2O Metabolic Incorporation in a Single Bacterium. *Adv. Sci.* **2020**, *7* (19), 2001452.
(90) Schiessl, K. T.; Hu, F.; Jo, J.; Nazia, S. Z.; Wang, B.; Price-Whelan, A.; Min, W.; Dietrich, L. E. P. Phenazine Production Promotes Antibiotic Tolerance and Metabolic Heterogeneity in Pseudomonas aeruginosa Biofilms. *Nat. Commun.* **2019**, *10* (1), 1−10.
(91) Bae, K.; Zheng, W.; Ma, Y.; Huang, Z. Real-Time Monitoring of Pharmacokinetics of Antibiotics in Biofilms with Raman-Tagged Hyperspectral Stimulated Raman Scattering Microscopy. *Theranostics* **2019**, *9* (5), 1348−1357.
(92) Meister, K.; Niesel, J.; Schatzschneider, U.; Metzler-Nolte, N.; Schmidt, D. A.; Havenith, M. Label-Free Imaging of Metal-Carbonyl Complexes in Live Cells by Raman Microspectroscopy. *Angew. Chemie - Int. Ed.* **2010**, *49* (19), 3310−3312.
(93) Bird, R. E.; Lemmel, S. A.; Yu, X.; Zhou, Q. A. Bioorthogonal Chemistry and Its Applications. *Bioconjugate Chem.* **2021**, *32* (12), 2457−2479.
(94) Scinto, S. L.; Bilodeau, D. A.; Hincapie, R.; Lee, W.; Nguyen, S. S.; Xu, M.; am Ende, C. W.; Finn, M. G.; Lang, K.; Lin, Q.; et al. Bioorthogonal Chemistry. *Nat. Rev. Methods Prim.* **2021**, *1* (1), 30.
(95) Saleh, A. M.; Wilding, K. M.; Calve, S.; Bundy, B. C.; Kinzer-Ursem, T. L. Non-Canonical Amino Acid Labeling in Proteomics and Biotechnology. *J. Biol. Eng.* **2019**, *13* (1), 1−14.
(96) Zhang, J.; Yan, S.; He, Z.; Ding, C.; Zhai, T.; Chen, Y.; Li, H.; Yang, G.; Zhou, X.; Wang, P. Small Unnatural Amino Acid Carried Raman Tag for Molecular Imaging of Genetically Targeted Proteins. *J. Phys. Chem. Lett.* **2018**, *9* (16), 4679−4685.
(97) Lampkowski, J. S.; Villa, J. K.; Young, T. S.; Young, D. D. Development and Optimization of Glaser-Hay Bioconjugations. *Angew. Chemie - Int. Ed.* **2015**, *54* (32), 9343−9346.
(98) Weerapana, E.; Wang, C.; Simon, G. M.; Richter, F.; Khare, S.; Dillon, M. B. D.; Bachovchin, D. A.; Mowen, K.; Baker, D.; Cravatt, B. F. Quantitative Reactivity Profiling Predicts Functional Cysteines in Proteomes. *Nature* **2010**, *468* (7325), 790−797.
(99) Backus, K. M.; Correia, B. E.; Lum, K. M.; Forli, S.; Horning, B. D.; González-Páez, G. E.; Chatterjee, S.; Lanning, B. R.; Teijaro, J. R.; Olson, A. J.; et al. Proteome-Wide Covalent Ligand Discovery in Native Biological Systems. *Nature* **2016**, *534* (7608), 570−574.
(100) Zanon, P. R. A.; Yu, F.; Musacchio, P. Z.; Lewald, L.; Zollo, M.; Krauskopf, K.; Mrdović, D.; Raunft, P.; Maher, T. E.; Cigler, M.; et al. Profiling the Proteome-Wide Selectivity of Diverse Electrophiles. *ChemRxiv* **2021**, DOI: 10.26434/chemrxiv.14186561.v1.
(101) Miao, Y.; Shi, L.; Hu, F.; Min, W. Probe Design for Super-Multiplexed Vibrational Imaging. *Phys. Biol.* **2019**, *16* (4), 041003.
(102) Zhuge, M.; Huang, K.-C.; Lee, H. J.; Jiang, Y.; Tan, Y.; Lin, H.; Dong, P.-T.; Zhao, G.; Matei, D.; Yang, Q.; Cheng, J.-X. Ultrasensitive Vibrational Imaging of Retinoids by Visible Preresonance Stimulated Raman Scattering Microscopy. *Adv. Sci.* **2021**, *8* (9), 2003136.
(103) Xiong, H.; Qian, N.; Miao, Y.; Zhao, Z.; Min, W. Stimulated Raman Excited Fluorescence Spectroscopy of Visible Dyes. *J. Phys. Chem. Lett.* **2019**, *10* (13), 3563−3570.
(104) Hu, F.; Zeng, C.; Long, R.; Miao, Y.; Wei, L.; Xu, Q.; Min, W. Supermultiplexed Optical Imaging and Barcoding with Engineered Polyynes. *Nat. Methods* **2018**, *15* (3), 194−200.
(105) Su, X.; Liu, R.; Li, Y.; Han, T.; Zhang, Z.; Niu, N.; Kang, M.; Fu, S.; Wang, D.; Wang, D.; Tang, B. Z. Aggregation-Induced Emission-Active Poly(Phenyleneethynylene)s for Fluorescence and Raman Dual-Modal Imaging and Drug-Resistant Bacteria Killing. *Adv. Healthc. Mater.* **2021**, *10* (24), 2101167.
(106) Lucotti, A.; Tommasini, M.; Fazzi, D.; Del Zoppo, M.; Chalifoux, W. A.; Tykwinski, R. R.; Zerbi, G. Absolute Raman Intensity Measurements and Determination of the Vibrational Second Hyperpolarizability of Adamantyl Endcapped Polyynes. *J. Raman Spectrosc.* **2012**, *43* (9), 1293−1298.
(107) Zeng, C.; Hu, F.; Long, R.; Min, W. A Ratiometric Raman Probe for Live-Cell Imaging of Hydrogen Sulfide in Mitochondria by Stimulated Raman Scattering. *Analyst* **2018**, *143* (20), 4844−4848.
(108) Wilson, L. T.; Tipping, W. J.; Jamieson, L. E.; Wetherill, C.; Henley, Z.; Faulds, K.; Graham, D.; MacKay, S. P.; Tomkinson, N. C. O. A New Class of Ratiometric Small Molecule Intracellular PH Sensors for Raman Microscopy. *Analyst* **2020**, *145* (15), 5289−5298.
(109) Tipping, W. J.; Wilson, L. T.; Blaseio, S. K.; Tomkinson, N. C. O.; Faulds, K.; Graham, D. Ratiometric Sensing of Fluoride Ions Using Raman Spectroscopy. *Chem. Commun.* **2020**, *56* (92), 14463−14466.
(110) Takemura, S.; Watanabe, H.; Nishihara, T.; Okamoto, A.; Tanabe, K. Monitoring Intracellular Metal Ion Complexation with an Acetylene-Tagged Ligand by Raman Spectroscopy. *RSC Adv.* **2020**, *10* (59), 36119−36123.
(111) Egoshi, S.; Dodo, K.; Ohgane, K.; Sodeoka, M. Deuteration of Terminal Alkynes Realizes Simultaneous Live Cell Raman Imaging of Similar Alkyne-Tagged Biomolecules. *Org. Biomol. Chem.* **2021**, *19* (38), 8232−8236.
(112) Bi, X.; Miao, K.; Wei, L. Alkyne-Tagged Raman Probes for Local Environmental Sensing by Hydrogen − Deuterium Exchange. *J. Am. Chem. Soc.* **2022**, *144*, 8504−8514.
(113) Shi, L.; Hu, F.; Min, W. Optical Mapping of Biological Water in Single Live Cells by Stimulated Raman Excited Fluorescence Microscopy. *Nat. Commun.* **2019**, *10* (1), 1−8.
(114) Lang, X.; Welsher, K. Mapping Solvation Heterogeneity in Live Cells by Hyperspectral Stimulated Raman Scattering Microscopy. *J. Chem. Phys.* **2020**, *152* (17), 174201.
(115) Lee, H. J.; Huang, K. C.; Mei, G.; Zong, C.; Mamaeva, N.; Degrip, W. J.; Rothschild, K. J.; Cheng, J. X. Electronic Preresonance Stimulated Raman Scattering Imaging of Red-Shifted Proteorhodopsins: Toward Quantitation of the Membrane Potential. *J. Phys. Chem. Lett.* **2019**, *10* (15), 4374−4381.
(116) Tang, Q.; Liu, L.; Guo, Y.; Zhang, X.; Zhang, S.; Jia, Y.; Du, Y.; Cheng, B.; Yang, L.; Huang, Y. Optical Cell Tagging for Spatially Resolved Single Cell RNA Sequencing. *Angew. Chem., Int. Ed.* **2022**, *61*, e202113929.